SPATIO-TEMPORAL DYNAMICS OF SENSORIMOTOR TRANSFORMATIONS IN MOUSE DORSAL CORTEX

Inauguraldissertation
zur Erlangung der Würde eines Doktors der Philosophie
vorgelegt der
Philosophisch-Naturwissenschaftlichen Fakultät
der Universität Basel

von

Ivana Orsolic
aus Kroatien

2020.

Genehmigt von der Philosophisch-Naturwissenschaftlichen Fakultät auf Antrag von

Prof. Dr. Thomas Mrsic-Flogel
Prof. Dr. Jan Gründemann

Basel, den 19.11.2019.

_____
Prof. Dr. Martin Spiess
Dekan

Table of Contents

Acknowledgements

I would like to thank my supervisor, Prof. Thomas D. Mrsic-Flogel, for the opportunity to perform research in the excellent setting of his laboratory. I am tremendously grateful for the freedom and the trust he gave me to pursue my research interests independently, and for his support throughout this time.

I would like to thank Dr. Georg Keller and Prof. Sonja Hofer for their valuable inputs and pastoral care as members of my PhD progress advisory committee.

I would like to thank the amazing lab members, both in Basel and London, for the comradery we shared in research, and for filling often isolating academic life with friendships and precious moments.

I would like to thank Dr. Kelly B. Clancy for our discussions about academia and science in general. Being a first-generation graduate, I have found these interactions most valuable.

To my family for their support and sacrifices - thank you for instilling love for learning and fearlessness about the unknown.

Finally, I would like to thank my husband Petr for his endless support, and for giving me confidence, both professionally and personally, to put myself and my research forward.

List of figures

List of abbreviations

VISp – Primary visual area (mouse)

VISpm – Posteromedial visual area

VISam – Anteromedial visual area

VISa – Anterior area

VISrl – Rostrolateral visual area

VISal – Anterolateral visual area

VISli – Laterointermediate area

VISl – Lateral visual area

RSPagl – Retrosplenial area, lateral agranular part

RSPd – Retrosplenial area, dorsal part

RSPv – Retrosplenial area, ventral part

ACAd – Anterior cingulate area

FRP – Frontal pole, cerebral cortex

PL – Prelimbic area

MOs – Secondary motor area

Mop – Primary motor area

SSs – Supplemental somatosensory area

SSp-bfd – Primary somatosensory area, barrel field

SSp-ll – Primary somatosensory area, lower limb

SSp-m – Primary somatosensory area, mouth

SSp-n – Primary somatosensory area, nose

SSP-tr – Primary somatosensory area, trunk

SSP-ul – Primary somatosensory area, upper limb

SSP-un – Primary somatosensory area, unassigned

MT – Middle temporal visual area

LIP – Lateral intraparietal area

ALM – Anterior lateral motor area

CCF - The Allen Mouse Common Coordinate Framework

ROI – Region of interest

CI – Confidence intervals

Chapter 1. Introduction and overview

1.1. Background and literature review

Studying how animals use sensory information in the environment to produce relevant actions is one of the central questions of neuroscience. These sensorimotor transformations are often studied in the context of decision-making where perceptual tasks are often employed to infer the link between sensation and action (Gold and Shadlen 2007), providing a handle on the neural correlates of sensory-motor transformations. At the time of writing this thesis, neuroscience is in the era when it is feasible to obtain rich and large datasets of neural activity from the behaving brain and the way behaviour is used in neuroscience becomes an important topic of debate (Mobbs *et al.* 2018, Tye and Uchida 2018, Babayan and Konen 2019). On one hand, there is criticism that the perceptual tasks used can be very unnatural and disregard animals' ecology, viewing them as function machines (Krakauer *et al.* 2017, Gomez-Marin and Ghazanfar 2019). Training animals in trial-based paradigms with arbitrary associations between the stimuli and actions may not reveal how the brain operates in its natural conditions because processes studied might be fundamentally different. For example, most perceptual tasks often focus on distinct and rapid periods of decision-making ignoring neural processes that occur on longer timescales (Huk *et al.* 2018). On the other hand, such "reductionism" in behaviour is necessary in order to maintain the experimental control and data interpretability (Hanks and Summerfield 2017, Juavinett *et al.* 2018, Waskom *et al.* 2019) echoing the challenges of studying processes in which underlying computations may involve latent cognitive variables

that need to be isolated from a plethora of continuously ongoing, and often correlated, processes that naturally occur in the brain of a behaving subject.

Success, or at least best attempts, at designing a tractable approach for understanding the neural underpinnings of cognitive processes crucially depends on the design of behavioural tasks, keeping in mind the compatibility of the method used with the biological question and biological system studied. That means moving from the short and rigid trial structure to studying ongoing input-output processes and the associated neural responses on longer timescales without compromising the interpretability of the data (Huk *et al.* 2018).

1.1.1. Neural corelates of decision-making elements in primates: from representation of stimulus to representation of choice

Probing for neural correlates of decision-making has its origins in awe-inspiring work in primates using perceptual tasks involving working memory (Werner and Mountcastle 1965, Mountcastle *et al.* 1990) and discrimination of motion direction (Newsome and Pare 1988). Some of the earliest work focused on the sensory representations that guide the perceptual decisions, showing that the firing rates of neurons in sensory areas correlate closely with the psychophysical performance of the subject, linking neurophysiology and psychophysics together (Newsome *et al.* 1989, Mountcastle *et al.* 1990, Britten *et al.* 1993, 1996, Hernandez *et al.* 2000). Furthermore, the sensory evidence artificially introduced via microsimulation could be used by the subjects in the same way as the evidence transmitted via regular mechanical or visual stimulation of peripheral sensory receptors (Salzman *et al.* 1990, Romo *et al.* 1998, 2000). Exciting follow up work characterised involvement of an

array of brain areas and reported that the neural representations along the sensorimotor axis evolve from being strongly correlated with the stimulus strength in sensory areas to being strongly corelated with the performance of the subject in the prefrontal cortex (Kim and Shadlen 1999, Hernández *et al.* 2002, de Lafuente and Romo 2006).

In the motion discrimination task (Newsome and Pare 1988, Newsome *et al.* 1989) monkeys were trained to discriminate the net motion direction of the visual stimulus. The reaction-time based version of this task (Roitman and Shadlen 2002) allowed monkeys to interrupt the trial and answer without the imposed temporal delay of the fixed-duration version of the task. The absence of this delay made it possible to quantitatively characterize the relationship between the sensory evidence and motor action as not only the choice, but the time it took to reach the choice was now known. If monkeys were integrating observed motion until the decision was made, weaker motion would require longer integration time, resulting in longer reaction times. It was now possible to attribute the "quality" or the "weight" to the sensory evidence used in decision-making, and the effect it exerts on firing rates and animals' behaviour (Gold and Shadlen 2001, 2002, Mazurek *et al.* 2003). Activity of the area LIP, an area of parietal cortex implicated in the saccade selection, exhibited ramp-like activity, dependent on the stimulus strength, that culminated around the time the choice was produced (Roitman and Shadlen 2002). Furthermore, activity of LIP neurons was modulated by pulses of stronger motion evidence injected into the ongoing stimulus, which produced an elevation in firing rate lasting up to 800 ms after the pulse has elapsed (Huk and Shadlen 2005). However, recent work has challenged the idea that this area plays a causal role in evidence accumulation (Katz *et al.* 2016) and demonstrated that the activity of other areas can reflect evidence accumulation process

as well (Shadlen and Newsome 1996, Kim and Shadlen 1999, Ding and Gold 2010, Siegel *et al.* 2015).

These results highlighted the need for an unbiased and precise characterisation of many brain areas during decision-making in order to discover their distinct roles in this process.

1.1.2. Using mice in studying and mapping of neural circuits of decision-making

The approach pioneered in primates has been long held as the gold standard for studying decision-making due to the ability to exploit complex tasks with parametrised stimuli and controlled motor output of the subject. After the distributed nature of neural correlates of decision-making was revealed by primate studies (Hernández *et al.* 2010, Siegel *et al.* 2015), future experiments required tools employable in genetically accessible subjects to manipulate and capture activity on larger scales in order to disentangle these distributed circuits.

Mice are genetically tractable and are an excellent candidate model for this approach (Huang and Zeng 2013, Luo *et al.* 2018). Mice and rodents in general are becoming more represented in the field of perceptual decision-making (Carandini and Churchland 2013). Mice have been shown to be able to discriminate between stimuli regardless of modality of the stimulus or the motor output (Huber *et al.* 2008, Andermann *et al.* 2010, O'Connor *et al.* 2010, Sanders and Kepecs 2012, Guo *et al.* 2014, Hangya *et al.* 2015, Poort *et al.* 2015, Burgess *et al.* 2017), and recently to accumulate sensory evidence (Odoemene *et al.* 2018, Pinto *et al.* 2018). Due to the methodological need of restricting the movements of the subject, mice are often head-

fixed in the behavioural apparatus while either restrained or allowed to run. In order to allow for naturalistic behaviours such as spatial navigation to be studied in head-fixed mice, mice are embedded in closed-loop environments where the optic flow is generated and linked to the mouse's running (Harvey *et al.* 2012, Keller *et al.* 2012, Pinto *et al.* 2018). However, careful consideration should be given when attributing neural activity to putative cognitive parameters of the task in paradigms where motor output correlates with those parameters (Krumin et al. 2018, Pinto et al. 2019). To avoid these potential confounds animals are often physically restrained during the task.

To date, circuit mechanisms of perceptual decision-making in mice have been most exhaustively approached from the perspective of motor planning in a tactile discrimination task, where physically restrained mice were asked to withhold a response about the location of the stimulus (Guo et al. 2014). This work also serves as the demonstration of how powerful the mouse is as a model in probing the neural circuits of perceptual decision-making. During the task authors inactivated dozens of cortical areas during two distinct epochs of the trial – during sensory stimulation and during the delay period prior to action – and argued for a serial scheme of decision making, where information flows from sensory to motor areas with little temporal overlap (Guo *et al.* 2014). Optogenetic silencing of a motor area involved in licking behaviour (ALM) during the delay did not produce a motor deficit, but instead biased the mouse licking to the side ipsilateral to the perturbation (Guo *et al.* 2014). The animals' eventual choice could be decoded from the activity of ALM neurons during the delay period - suggesting a role in motor preparation, as well as during the licking period - suggesting a role in execution of the behavioural choice (Guo *et al.* 2014). Further work attributed the two roles of ALM to distinct circuits dependent on different classes of deep layer pyramidal cells (Li *et al.* 2015, Economo *et al.* 2018).

In addition, the persistent activity in ALM was shown not to be maintained locally but via thalamocortical loop (Guo *et al.* 2017), which later work expanded to include the cerebellum as well (Gao *et al.* 2018).

These results once again confirmed the distributed nature of perceptual decision-making, this time from the perspective of motor preparation.

1.1.3. Decision-making and motor planning: tomato – tomato or an important difference?

The division between decision-making and motor planning studies in mice stems from classical stimulus-transformation-action view. Decision-making studies primarily focus on epochs of stimulation and the effect of sensory evidence exerts on neural activity (Pinto *et al.* 2018, 2019). Motor planning is often studied in context of working memory, focusing on periods after the stimulation during which the animal is preparing the motor action (Guo *et al.* 2014, 2017, Li *et al.* 2015, Gao *et al.* 2018, Svoboda and Li 2018).

Sensory stimulation and action are often spatially and/or temporally severed by the design of the behavioural task itself. However, it is still unclear if the decision-making and motor preparation are implemented using different neural circuitry (Murakami and Mainen 2015, Svoboda and Li 2018). Alternative to the serial view of decision making is that both decision-making and motor preparation are part of the same ongoing sensory-cognitive-motor loop. There are strong stances for both views, on one side that the motor control is essentially decision-making (Wolpert and Landy 2012) and on the other that the movement generation should be separated to distinct domains, one that is perceptual (decision-making) and the one that is strictly motor

(Bennur and Gold 2011, Wong *et al.* 2015). In order to avoid confirmation bias in approaching this matter, choice of whether to allow the subjects to respond freely or withhold their response during a delay period, becomes an important element of the task design.

Earliest insight into mental processes of action and decision-making come from studying reaction times (Donders 1969). Reaction times can be influenced not only by sensory evidence - decision time, but by other non-decision time processes as well, such as sensory and motor delays (Okazawa *et al.* 2018). Imposing a long delay period after the fixed-duration stimulus presentation can lessen the effect of non-decision time, however this comes at the expense of obscuring the decision-times. Activity in the delay periods can still be influenced by other processes such as the effect of past trials (Hwang *et al.* 2017, Akrami *et al.* 2018) and motor preparation (Guo *et al.* 2014). Processes that lead to a decision are often conflated with processes related to the execution of the decision. Such overt motor outputs, task related or spontaneous, have recently been shown to produce strong and global neural events (Allen *et al.* 2017, Steinmetz *et al.* 2018, Musall *et al.* 2019, Stringer *et al.* 2019).

Having the subject respond freely during decision-making can offer more opportunities to quantify the relationship between the stimulus and the action. The challenge then lies in separating the processes leading up to the decision from processes that relate strictly to the execution of choice, which may dominate neural activity. In this thesis, I present a novel behavioural task in mice that aims to address this challenge and describe the distinct patterns of activity in the dorsal neocortex associated with the processing of sensory evidence and the execution of behavioural choices in this task.

1.2. Aims and outline of the thesis

The aim of this thesis is to capture ongoing sensory-motor transformations during decision-making by:

(I) establishing a behavioural paradigm where ongoing psychophysical interrogation of stimulus-action relationship can take place on long timescales.

(II) obtaining unbiased and continuous assessment of dorsal cortex engagement during sensory-motor transformations on long timescales free from activity related to motor output.

Chapter 2 describes the development of a novel perceptual task aimed to separate processes leading to a choice from processes linked strictly to its execution. *Chapter 3* describes the development of the widefield calcium imaging setup, pre-processing of widefield signals and application of brain registration. *Chapter 4* describes the engagement of dorsal cortex during ongoing deliberation process in the absence of overt movements, *Chapter 5* describes the engagement of dorsal cortex during the ongoing deliberation process where animals' movement was not controlled, and during the execution of choice and other task-related motor actions. *Chapter 6* describes the influence of temporal expectation on the engagement of

dorsal cortex during the ongoing deliberation process in the absence of overt movements.

Chapter 7 offers Conclusions and perspectives and *Chapter 8* details the methodology.

1.3. Disclosures

The experiments described here were carried out by me in the lab and under the supervision of Prof. Thomas Mrsic-Flogel. Additional guidance on experimental design and data analysis was provided by Dr. Petr Znamenskiy.

Lisa Hoerman helped with animal training, Fabia Imhof and Lisa Hoerman helped with anatomy experiments. Dr. Robert Campbell provided code and assisted with brain registrations. Dr. Adil Khan assisted with circuit diagrams for components controlling the behavioural setup and with code for the finite state machine used in the control of the behavioural task.

All the results discussed in this thesis and the methods chapter have been made available online as part of the preprint, and were authored and produced by me:

Orsolic, **I**., Rio, M., Mrsic-Flogel, T.D., and Znamenskiy, P., 2019. Mesoscale cortical dynamics reflect the interaction of sensory evidence and temporal expectation during perceptual decision-making. *bioRxiv*, 552026,

Chapter 2. Visual change detection task as paradigm to study pre-decision processes

2.1. Behavioural task design

We developed a novel behavioural paradigm that aimed to separate the processes of decision making, during which the animals' behaviour is presumably still influenced by sensory evidence, from processes that occur when animal reported its choice or performed other task related or task unrelated overt movements.

2.1.1. Trial structure and stimulus design

We developed a visual change-detection reaction time paradigm where head-fixed animals (Figure 1) were trained to detect a sustained increase in the speed ("change") of a constantly fluctuating grating stimulus ("baseline") (Figure 2). By controlling the time of change, we introduced long baseline periods during which we measured neural activity underlying decision-making processes. Animals had to remain stationary to initiate a trial and during the baseline stimulus (11130 trials, 47 sessions, 6 mice).

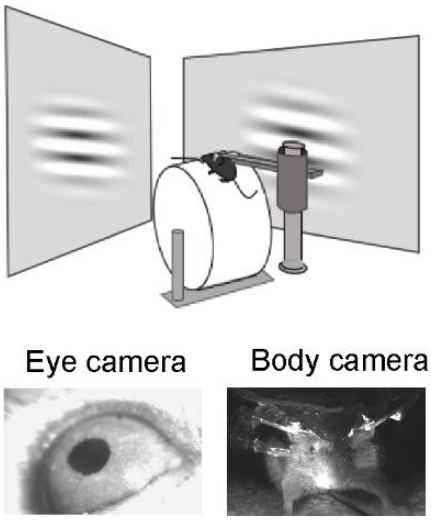

Figure 1. Behavioural setup and cameras for tracking overt behaviour.

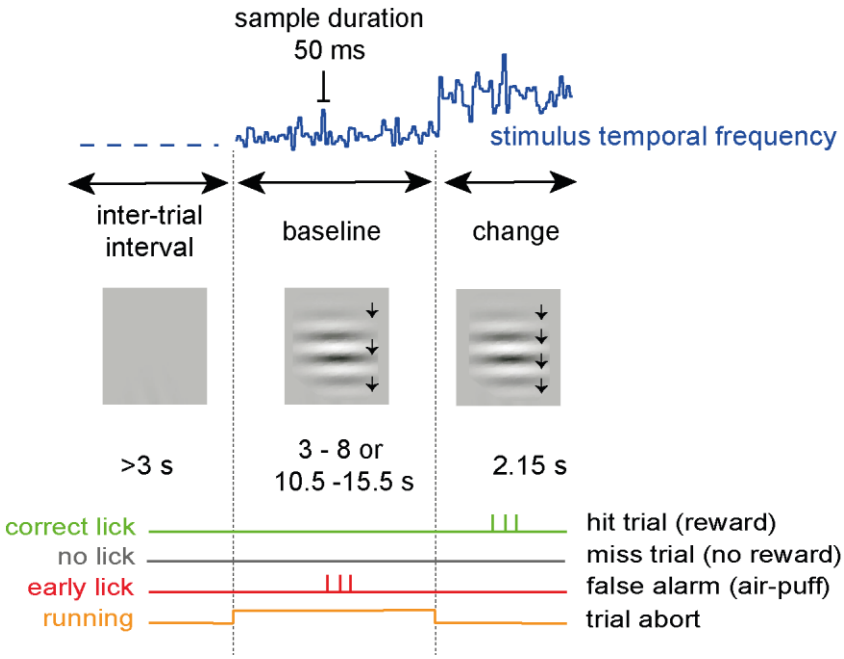

Figure 2. Structure of the behavioural task. The trial was divided to three epochs: intertrial interval, baseline period and change period. The onset of the drifting grating stimulus occurred once the animal was stationary (no running present) for a variable time period (minimum 3 s). A new stimulus sample was presented to the animal every 50 ms. After a randomized period, temporal frequency of the stimulus would change, and the mice were trained to detect this change to get a reward (correct lick). If the mouse licked (early lick) or moved (exhibited running) during the baseline period, the trial was classified as a false alarm or an abort, retrospectively.

In the initial version of the task, animals could run freely on the wheel (82005 trials, 281 sessions, 6 mice). After we observed that the running behaviour itself was modulated by the stimulus fluctuations, we modified the task such that animals had to voluntarily remain stationary during the baseline period. This was to ensure that the neural activity measured during the baseline stimulus was free from the modulations associated with the motor execution of choice or other movements. Performance and neural responses during the running version of the task will be presented and discussed separately in Chapter 5, providing a contrast to task-elicited neural responses in the version where mice remained stationary (Chapter 4 and Chapter 6).

To encourage animals to remain attentive during this baseline period we introduced several elements to the task design. The changes in stimulus speed were *ambiguous* - the animals could not ignore small stimulus fluctuations as the amplitude of change of the trial animal was currently in was unknown and the smallest stimulus changes overlapped in amplitude with the pre-change stimulus fluctuations. *Time of change was randomized* within a change block with a flat change hazard rate during the period where changes were likely. These elements encouraged the animals to make their choices based on multiple stimulus samples in order to correctly detect the sustained increase in the stimulus speed. On the other hand, to encourage animals to respond to the change as soon they had detected it the window to report the change was limited (1.15 s for running mice and 2.15 s for stationary mice).

Each trial began with a grey isoluminant screen during which the animal had to observe running requirements (stationary vs. running). After a randomized delay period (3 s + a sample from an exponential distribution with the mean of 0.5 s), the baseline stimulus appeared (sinusoidal grating with the spatial frequency of 0.04 cycles per degree, square patch of ~75 degrees). The temporal frequency of the

baseline stimulus increased after a randomized baseline - pre-change period duration, whose distribution varied in blocks (early block: 3-8 seconds, late block: 10.5-15.5 seconds). On the majority of trials, the temporal frequency of the grating was drawn every 50 ms (3 monitor refresh frames) from a lognormal distribution, such that $\log_2$-transformed TF had the mean of 0 (i.e. geometric mean TF of 1 Hz) and standard deviation of 0.25 octaves. These extended periods of baseline fluctuations in speed enabled us to observe the moment-to-moment influence of stimulus samples on neural activity and to manipulate task statistics and probability of change on long timescales. In a subset of trials (30%) no noise was added and baseline stimulus had a constant TF of 1 Hz. In 20% of trials the change did not occur, and no reward was given.

Mice reported the increases in the stimulus speed by licking the spout presented to them in order to trigger reward delivery, a drop of soy milk. If the animal licked before the change occurred ("early lick", false alarm trials 3590/19734 trials), the trial was aborted, and a gentle air-puff was delivered to the right cheek of the animal as feedback. In case the mice did not lick within the 2.15 second response window following the change (miss trial) the trial ended without the reward. If mice licked within 0.15 s after the speed change ('refractory licks'), no reward or air-puff was given, and these trials (58/19734 trials) were excluded from analysis as they were not likely to have occurred in response to the change.

2.2. Psychophysical performance and psychophysical reverse correlation

Animals' performance in this task was dependent on the strength of the sensory evidence that indicated to the animal that the change in stimulus speed has indeed occurred (i.e. magnitude of speed change, Figure 3). Animals detected lager changes at a higher rate and with shorter reaction times (Figure 3B-D). This relationship between the magnitude of stimulus speed and behavioural responses could mean that the mice were integrating over several stimulus samples in order to detect the change or could employ an alternative random sampling strategy given that the baseline period was constant from trial to trial.

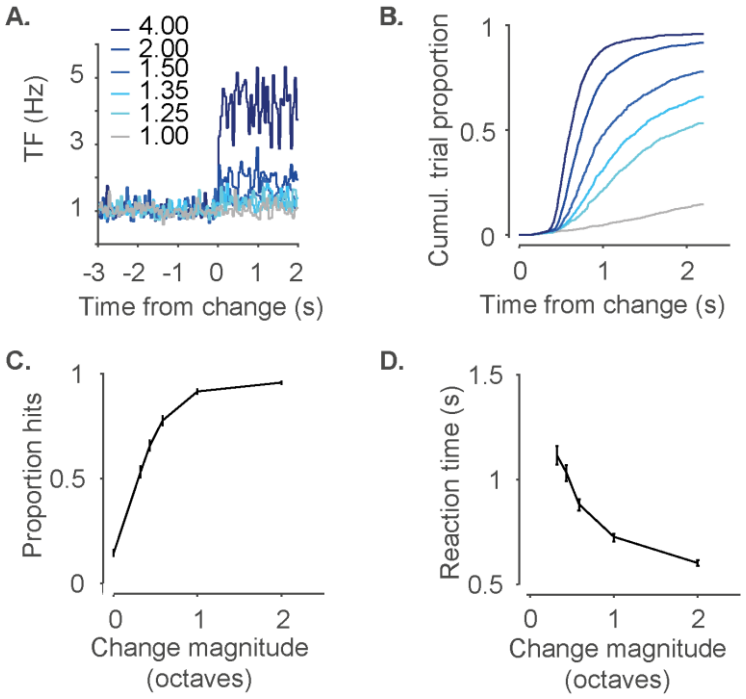

Figure 3. Mouse performance in the task. A. Trial difficulty was controlled by changing the strength of change. **B.** Cumulative trial proportion of reaction times across the change strength. Mouse detection rate **C.** and the reaction times **D.** were dependent on the strength of the stimulus change.

Examination of stimulus content prior to the early licks suggest that the licking behaviour during the baseline period was influenced by the fluctuating stimulus speed. Psychophysical reverse correlation revealed an increase in stimulus speed prior to the lick (Figure 4). If mice licked randomly, given the stochastic nature of the stimulus the kernel would appear flat around the mean stimulus value during the baseline period. The increase in stimulus speed lasting from 1 to 0.2 second before the lick indicates that the stimulus in this temporal window influences behaviour. However, this window can be distorted by sensory and motor delays and cannot provide exact stimulus-behaviour relationship (Okazawa *et al.* 2018).

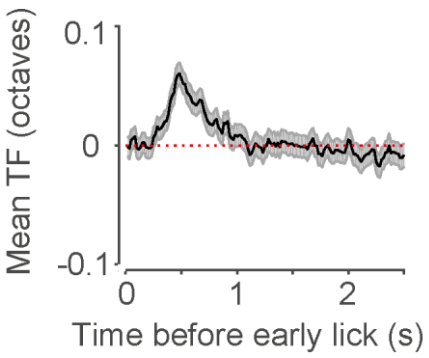

Figure 4. Psychophysical reverse correlations. Average stimulus preceding licks during the baseline stimulus (n=6 mice, shading is 95% CI, red: average stimulus during the baseline period).

Licks were also not uniformly distributed during the timecourse of the baseline fluctuations. The hazard rate of the stimulus changes that mice experienced (Figure 5B) influenced the timing of the early licks (Figure 5C). Early lick hazard rate was elevated at the start of the trial in early blocks, when changes were more frequent. Expectation of when changes might occur also influenced the animals' detection

performance as mice were faster to respond to the most difficult change if the change was expected (Figure 5D).

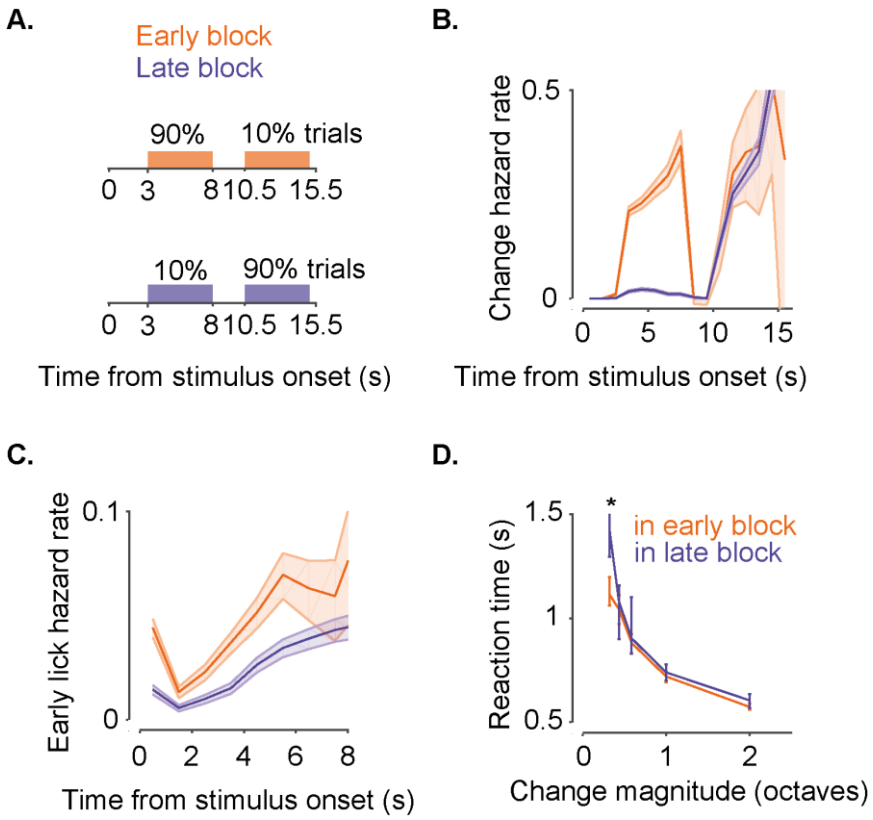

Figure 5. **Mouse behaviour is modulated by the anticipation of change. A.** Timing of change was varied in blocks where changes occurred either early (3-8s) or late (10.5-15.5s) relative to the trial onset. **B.** Probability of changes as function of time (hazard rate) in early and late blocks. **C.** Early lick hazard rate is modulated by anticipation of change. **D.** At low change magnitudes, responses to early changes (3-8 s after stimulus onset) are slower in late blocks, when changes are not expected (* – $p < 0.01$, Wilcoxon rank sum test).

2.3. Discussion

We aimed to experimentally deconstruct behaviour during ongoing decision-making processes where the animal's choice is still influenced by sensory evidence from behaviours strictly associated with reporting the choice such as licking, reward consumption or other overt movements. To achieve this, we created a task epoch during which the animal remains attentive to the stimulus fluctuation (baseline period) that is well separated from the epoch in which the animal reaches and executes the decision (change period). Furthermore, we expanded the baseline period duration (3 – 15.5 s), to observe neural processes on timescales that are typically left unexplored in decision-making paradigms.

We observed a clear relationship between the strength of the evidence and the animals' behaviour both in terms of the detection rate and the reaction times. Chronometric and psychometric curves changed monotonically with the strength of sensory evidence. Animals' detection rate increased with stimulus speed, while the reaction times decreased with the increase in change magnitude (Figure 3C,D). The latter observation suggests that the mice might be employing an integration strategy in order to detect the mean of the fluctuating stimulus speed. Psychophysical reverse correlation supports this suggestion and highlights the epoch and magnitude of the stimulus speed that is contributing to animals' behaviour. However, the relationship between the stimulus and the behaviour shown in psychophysical kernels is likely to be distorted due to sensory and/or motor delays (Okazawa *et al.* 2018). Alternative strategies such as random sampling can still be possible. Further analysis of animals' choices during the baseline stimulus revealed that the expectation of change also influenced animals 'behaviour: mice were more likely to respond to the stimulus with

the same statistics when the change was expected, compared to the period when the change is not likely.

Our task design provides extended periods in which to observe decision-making processes that are free from execution of choice while still preserving the stimulus-action relationship of the reaction-time paradigms. The rate and timing of correct licks following the change period suggest that the animals' choices were influenced by the "quality" of the sensory evidence in favour of the change, while the early licks before the change reveal that the small stimulus fluctuations are enough to drive the animals' licking behaviour. The animals' licking behaviour was further influenced by not only *current* sensory evidence coming from these baseline fluctuations, but by the *past* history of changes that the animal had experienced as well.

Chapter 3. Widefield calcium imaging

3.1. Imaging setup design and acquisition parameters

To systematically characterise the activity of dorsal cortex during sensorimotor transformations that take place in our task, we built a custom-built tandem-lens epifluorescence macroscope for calcium imaging (Ratzlaff and Grinvald 1991) (Figure 6).

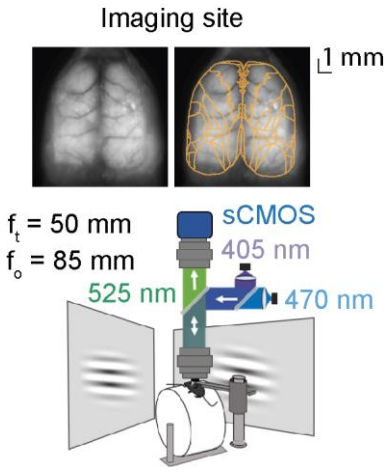

Figure 6. Widefield calcium imaging setup and the imaging site.

We imaged transgenic mice that expressed the calcium indicator GCaMP6s in excitatory populations (Wekselblatt et al., 2016) through the intact chronic skull preparation (Silasi *et al.* 2016). To ensure homogenous excitation throughout the imaging site, we delivered excitation in the Koehler configuration. Average power delivered to the imaging site was ~0.05 mW/mm^2, similar to that used in other studies (Wekselblatt et al. 2016). Images were acquired at ~20 µm per pixel and were further binned resulting in 170 µm per pixel final resolution. We recorded the onset of each

stimulus frame using a photodiode attached to the screen in order to ensure precise temporal alignment of stimulus samples and the imaging frames. Both acquisition and saving of acquired frames were stable throughout the recordings as confirmed by the post-hoc inspection of each session.

3.2. Haemodynamic correction

Metabolic activity of the tissue affects its optical properties (Grinvald *et al.* 1976, Ma *et al.* 2016) which can result in changes in florescence during imaging. To correct for these changes, we excited the calcium indicator with dual wavelength excitation at 470 nm and 405 nm that allowed us to correct for haemodynamic components of the signal (Allen *et al.* 2017). A microcontroller was used to controll the excitation onset triggered by the camera exposure output, interleaving excitation at each wavelength. Illumination was restricted to periods when all the lines of the frames were being acquired. Emitted fluorescence was passed through a band-pass filter (525/50 nm) and was acquired using an sCMOS camera at 50 Hz, yielding an imaging rate of 25 Hz for each excitation wavelength. The magnitude of the haemodynamic signals varied across cortical areas, matching the non-corrected signals in visual sensory areas (Figure 7). The corrected signal was produced by taking the ratio of signals acquired with 470 nm and 405 nm excitation respectively, that was then normalized by the mean of the ratio:

$$F(t) = \frac{F_{470}(t)/F_{405}(t)}{\frac{1}{N}\sum_{k=1}^{N} F_{470}(k)/F_{405}(k)}$$

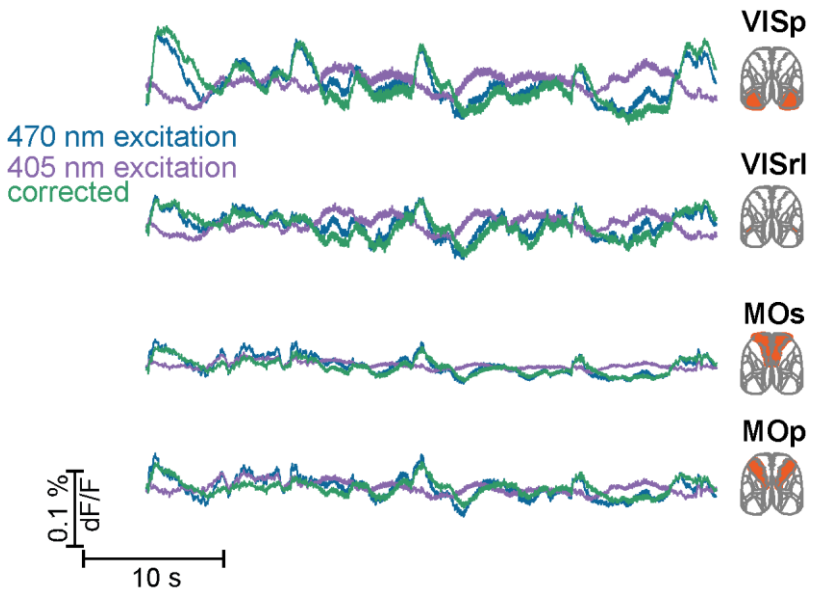

Figure 7. Hemodynamic correction of widefield signals. Example of recorded fluorescence signals with 470 nm and 405 nm excitation wavelength, and the fluorescence signal after removing haemodynamic component.

3.3. Registration of imaged brains within and across mice

All imaging sessions from individual mice were aligned to a reference imaging session using the vasculature pattern of the brain surface (Figure 8, Registration step 1). To compare data across mice, we imaged brains ex-vivo and aligned them to the Common Coordinate Framework provided by the Allen Institute for Brain Science (CCF, v.3 © 540 2015 Allen Institute for Brain Science, Allen Brain Atlas API, available from http://brain-map.org/api/index.html). Brains were coronally sectioned (100 µm steps) and imaged at two optical planes per one physical section using a custom serial two-photon tomography microscope (Figure 8, Registration step 2), resulting in a voxel size of 1.32 µm x 1.32 µm x 50 µm. After illumination correction

and stitching, brain volumes were registered to the CCF using Elastix (Klein *et al.* 2010) by applying rigid affine transformation followed by non-rigid deformation as described in (Han *et al.* 2018).

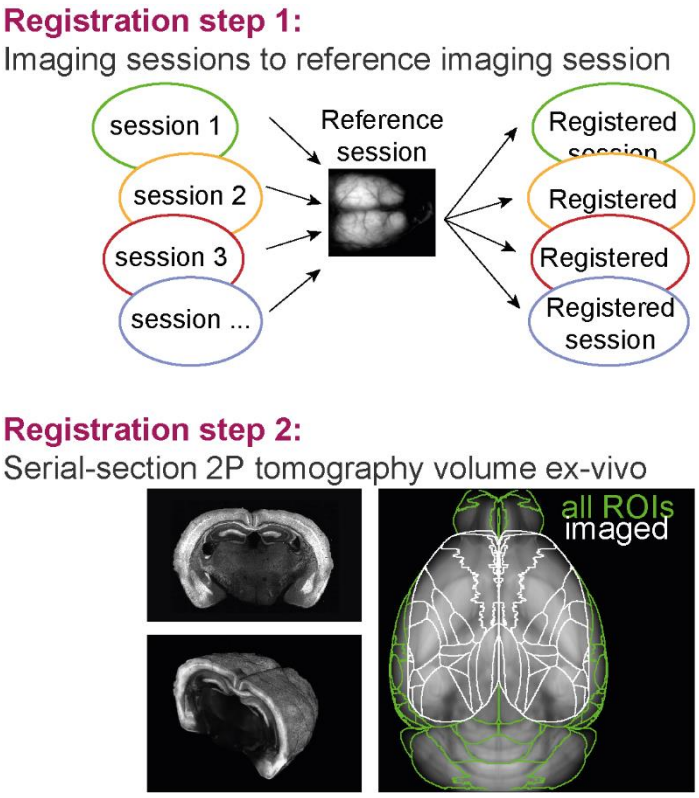

Figure 8. Registration of imaging sessions across mice and registration of ex-vivo data to the Allen Mouse Common Coordinate Framework. All imaging sessions from each subject were aligned to a single reference session using the vasculature pattern (**Registration step 1)** Brains were imaged ex-vivo and aligned to the Common Coordinate Framework provided by the Allen Institute for Brain Science (**Registration step 2**).

We reconstructed the superficial blood vessel pattern from serial two-photon tomography volumes using the fluorescence of the voxels near the brain surface (Figure 9, Registration step 3).

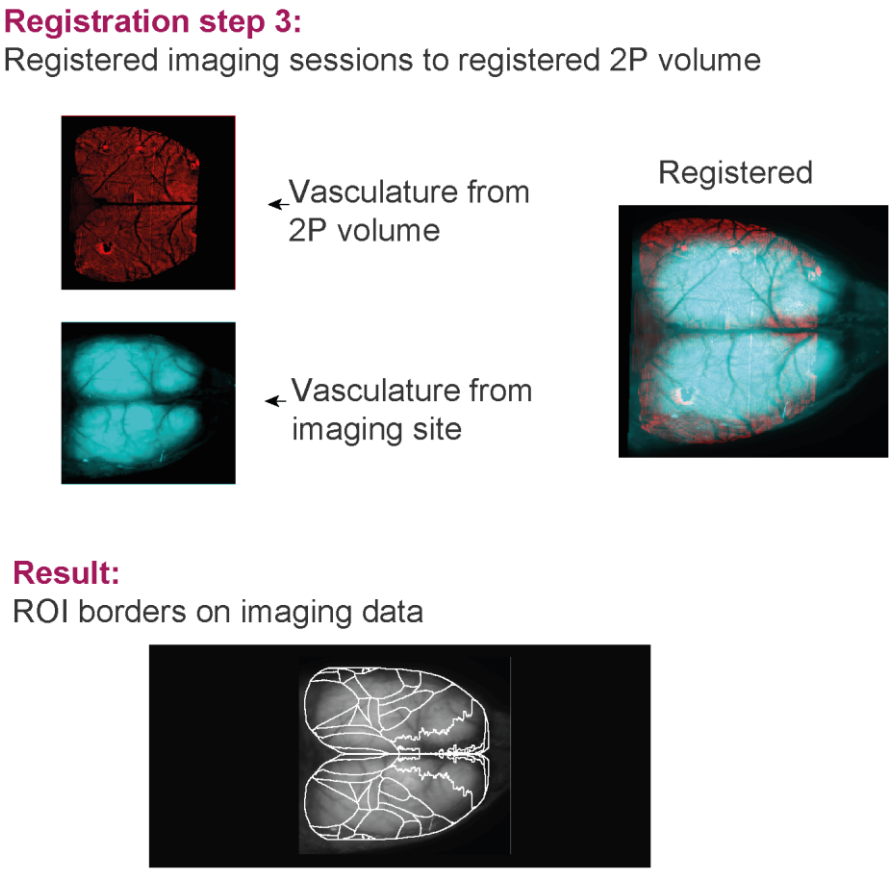

Finally, we aligned the imaging sessions registered within a subject to the ex-vivo imaged brain using the vasculature patterns of the reference imaging session. This transformed the imaging data from subject coordinates to the Common Coordinate Framework (Figure 9 - Result, Figure 10).

Figure 9. Registering imaging sessions to the Allen Mouse Common Coordinate Framework. Registration step 3 - registered imaging sessions are registered to the ex-vivo volume, aligning the imaging data with the Common Coordinate Framework provided by the Allen Institute for Brain Science. **Result –** imaging site in the Common Coordinate Framework.

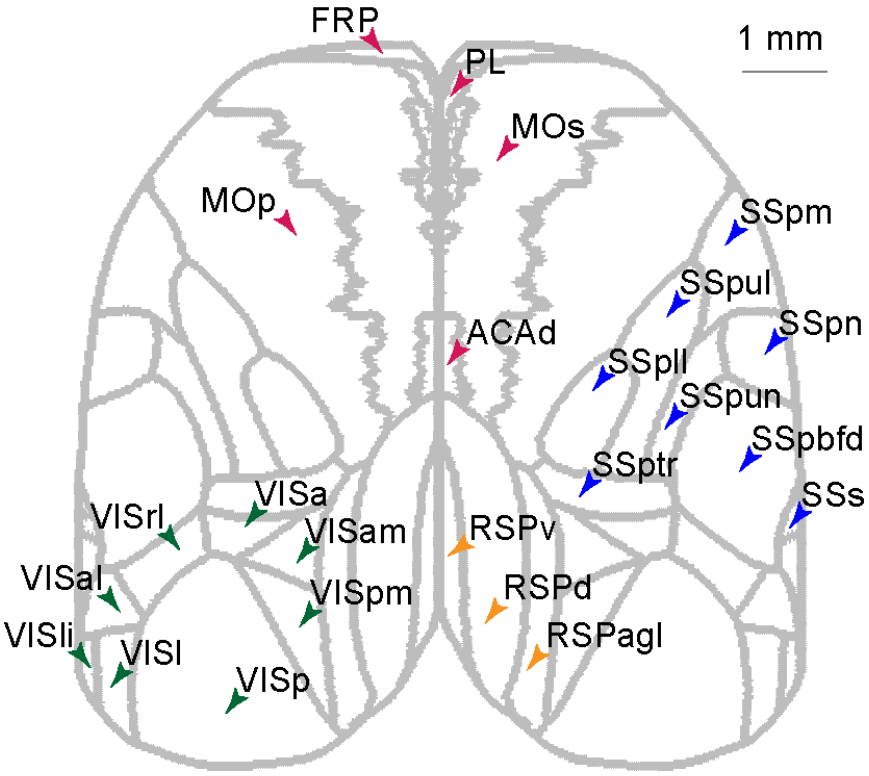

Figure 10. Identity of imaged cortical areas based on the Common Coordinate Framework provided by the Allen Institute for Brain Science.

VISp	Primary visual area
VISpm	Posteromedial visual area
VISam	Anteromedial visual area
VISa	Anterior area
VISrl	Rostrolateral visual area
VISal	Anterolateral visual area
VISli	Laterointermediate area
VISl	Lateral visual area
RSPagl	Retrosplenial area, lateral agranular part
RSPd	Retrosplenial area, dorsal part
RSPv	Retrosplenial area, ventral part
ACAd	Anterior cingulate area
FRP	Frontal pole, cerebral cortex
PL	Prelimbic area
MOs	Secondary motor area
Mop	Primary motor area
SSs	Supplemental somatosensory area
SSp-bfd	Primary somatosensory area, barrel field
SSp-ll	Primary somatosensory area, lower limb
SSp-m	Primary somatosensory area, mouth
SSp-n	Primary somatosensory area, nose
SSP-tr	Primary somatosensory area, trunk
SSP-ul	Primary somatosensory area, upper limb
SSP-un	Primary somatosensory area, unassigned

3.4. Discussion

We imaged transgenic animals expressing GCaMP6s in excitatory cells (Wekselblatt *et al.* 2016). This mouse line does not exhibit epileptiform activity as reported in some other transgenic lines (Steinmetz *et al.* 2017). As the method relies on detecting small differences in the fluorescent signals, the widefield signals can be contaminated by other processes that can affect the tissue reflectance and absorbance (Ma *et al.* 2016). Using the isosbestic wavelength to excite our calcium indicator (Lerner *et al.* 2015, Allen *et al.* 2017) we were able to isolate the widefield signal component that was dependent on the neural-activity induced changes in our calcium indicator.

Widefield signals are shown to arise from local populations rather from long-range projections (Makino *et al.* 2017), and are better correlated with the activity of superficial cortical layers (Allen *et al.* 2017), probably dendritic activity of cells in deeper layers. Even without providing single cell resolution, the widefield signals capture the average activity of the brain surface imaged and can therefore provide an unbiased macroscopic view of neural dynamics across the dorsal cortex, making wide-field imaging an important novel tool in decision-making studies (Allen *et al.* 2017, Makino *et al.* 2017, Zatka-Haas *et al.* 2018, Musall *et al.* 2019, Pinto *et al.* 2019).

Chapter 4. Dorsal cortex during ongoing evaluation of sensory evidence

4.1. Trial onset engages a global cortical network in trained mice

We aimed to characterise the engagement of the dorsal cortex while animals performed the task. First, we asked whether the trial onset engaged the activity of the dorsal cortex differently between the trained (6631 noisy trials > 1.5 seconds, 47 sessions, 6 mice) and naïve animals (1680 noisy trials 176 from 10 sessions in 3 mice) (Figure 11, Figure 12).

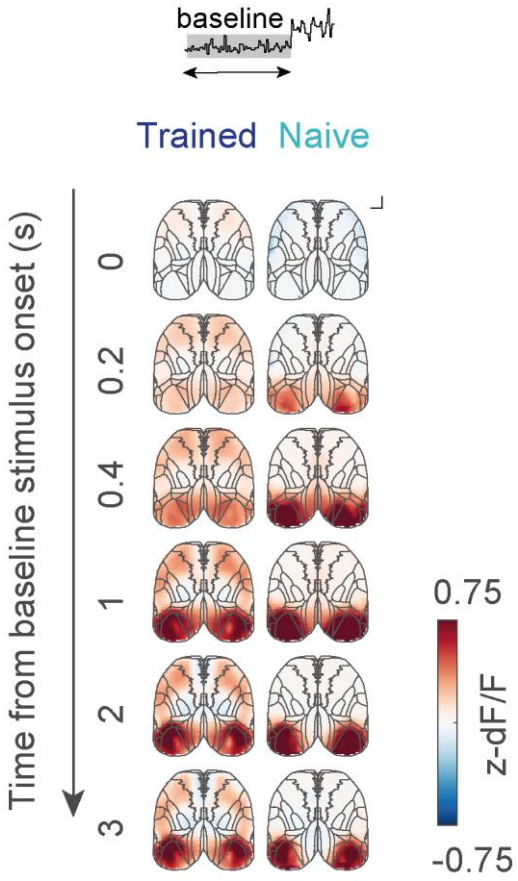

Figure 11. Stimulus onset broadly activates dorsal cortex in trained animals. Average z-scored stimulus response during the baseline stimulus period in trained (left, 6 mice) and naïve (right, 3 mice). Inset – shading indicates the analysed trial epoch. Scale bar – 1 mm.

In mice performing the task, grating onset triggered a sustained activation of primary and secondary visual areas followed by recruitment of secondary and primary motor cortex. While grating onset triggered responses of similar or even larger magnitude in visual areas in naïve mice, responses in motor areas were markedly weaker (Figure 12).

Thus, recruitment of motor cortex by the onset of the visual stimulus depends on animals' experience and occurs even in the absence of movement (Figure 12, bottom).

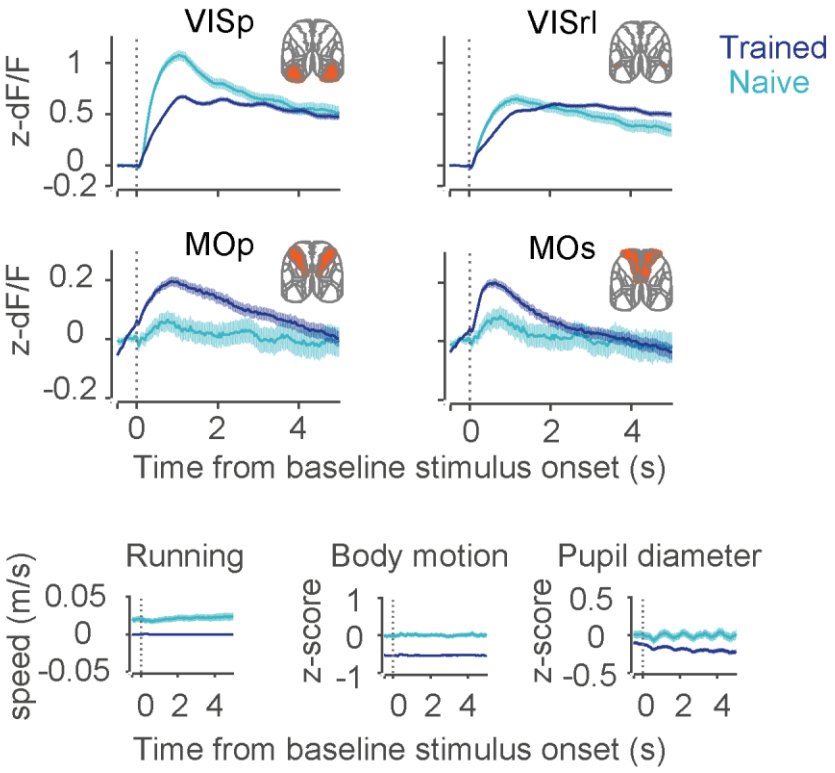

Figure 12. Responses to stimulus onset and progression across sensory and motor areas. Top: Mean z-scored responses of selected ROIs for trained and naïve animals. Vertical line marks the stimulus onset. Inset - shaded region corresponds to ROI shown. Bottom: Mean traces of running speed, body motion and pupil diameter for trained and naive animals.

4.2. Stimulus fluctuations produce spatio-temporally defined cascade of cortical activity

We used the prolonged movement-free baseline fluctuation period to characterize the relationship between the stimulus and neural activity during ongoing decision-making. This period was temporally well separated from the period where the animal reported its choice. Animals had to remain attentive to the baseline fluctuations to detect changes in the mean stimulus speed, amplitude and exact time of which varied from trial to trial.

4.2.1. Relationship and temporal progression of stimulus evoked modulation

In order to characterize cortical dynamics during decision-making, we used linear regression to quantify the influence of stimulus samples on cortical responses across different time-lags (Figure 13, 1039391 stimulus samples from 6894 trials in trained mice; 362291 stimulus samples from 1680 trials in naïve mice). This analysis included only baseline stimulus period during which the animals were stationary. If the trial was interrupted due to an early lick or movement, data preceding those events (1 second before) was excluded from the analysis. By fitting an multiexponential model to the regression coefficients, we characterised the timecourse of stimulus responses across cortical areas (half-max response latency and response decay time, respectively in Figure 14).

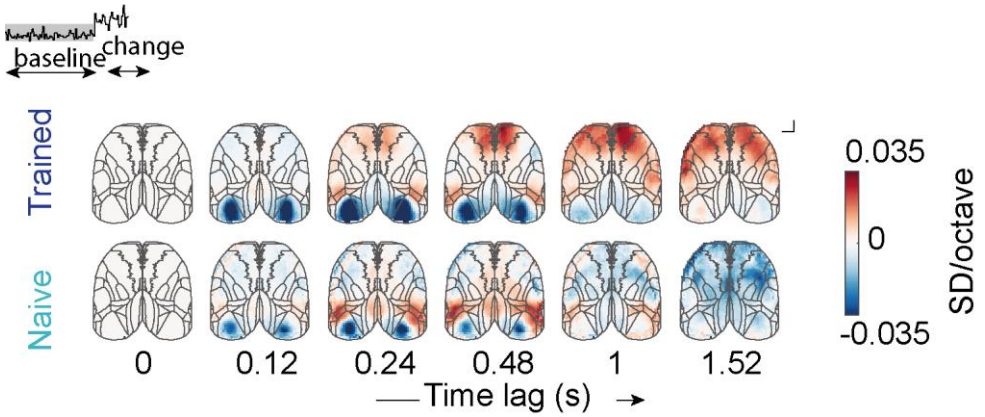

Figure 13. Differential modulation of cortical areas by stimulus between trained and naïve animals. Maps of regression coefficients of widefield fluorescence against baseline stimulus in trained (top) and naïve (bottom) animals across time lags. Inset – shading indicates the analysed trial epoch. Scale bar – 1 mm.

The shortest latencies (time until 50% of maximum response) were observed in visual sensory areas: primary visual cortex (VISp - 147 ms) and posteromedial higher visual area (VISpm - 159 ms), followed by other higher visual areas - rostrolateral visual area (VISrl - 209 ms), anterior visual area (VISa - 250 ms) and anterolateral visual area (VISal - 250 ms). Similar responses were also observed in naïve mice, consistent with their sensory-driven origins (Figure 13). The activity cascade continued with activation of secondary motor cortex (MOs - 333 ms), primary motor cortex (MOp - 632 ms) and somatosensory areas (lower and upper limb (SSp-ll, SSp-ul, 561-904 ms); nose and mouth (SSp-n, SSp-m, ~696-869 ms) (Figure 15). In contrast to responses in visual cortical areas, this part of the activity cascade was not observed in naïve mice (Figure 13).

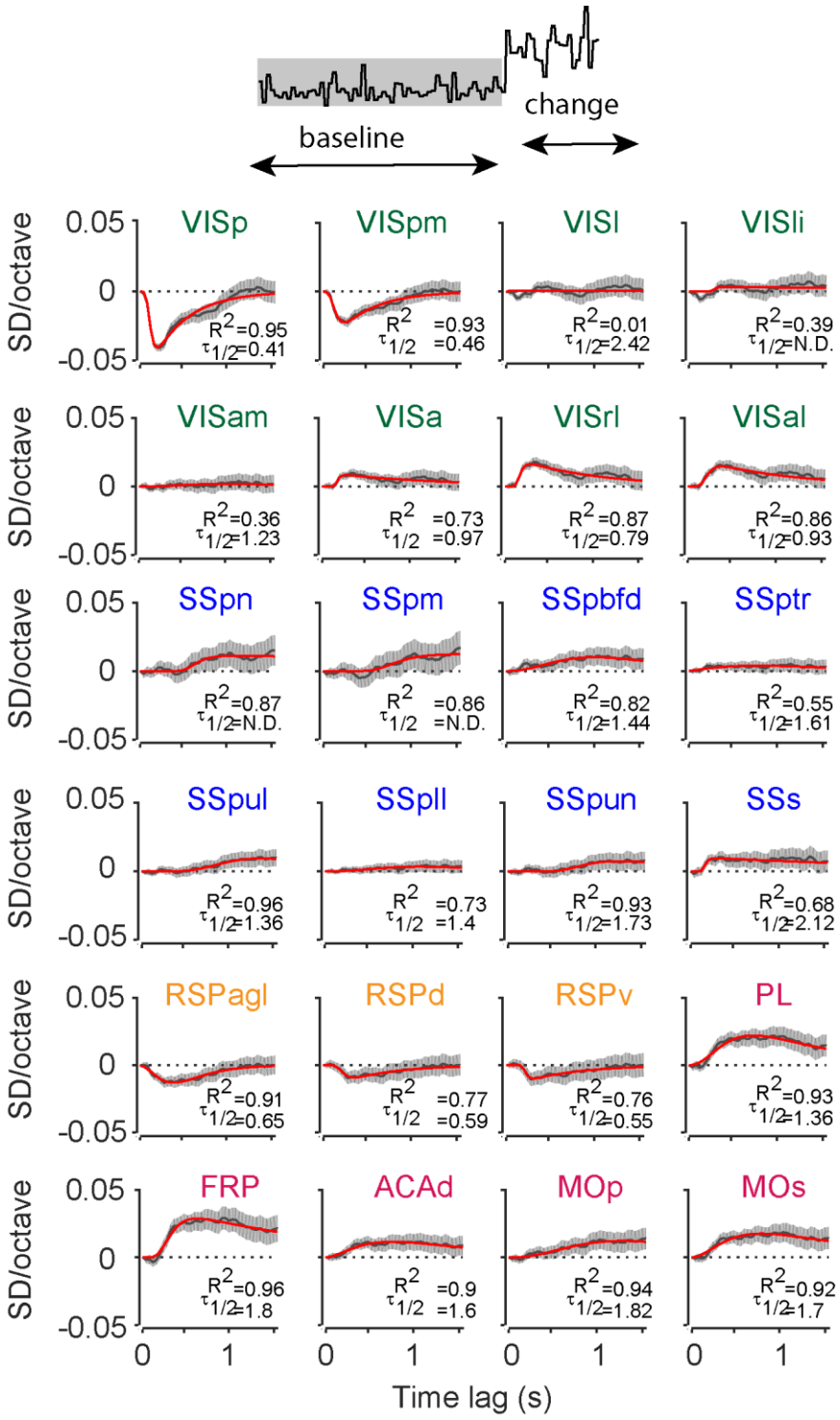

Figure 14. **Timecourse of stimulus responses across cortical areas.** Timecourse of regression coefficients of widefield fluorescence against baseline stimulus across all imaged ROIs; regression coefficients (gray 95% CI) and multiexponential fit (red). Inset – shading indicates the analysed trial epoch.

Cortical areas also varied in the decay time of the stimulus induced responses. Activity in primary visual cortex rapidly decayed to baseline (half-decay time of 410 ms), suggesting that it is largely modulated by the immediate history of sensory stimulation. In contrast, responses in higher visual areas were more sustained (VISrl – 790 ms, VISal – 930 ms, and VISa – 970 ms). In secondary and primary motor cortices half-decay times exceeded 1.5 s (MOs – 1700 ms, MOp – 1820 ms).

The decay time measurements are affected by the offset dynamics of the calcium indicator used. The fastest decay time we measured was 410 ms (in VISp), in good agreement with the reported half-decay time for somatic signals of GCaMP6s *in vivo* (Dana *et al.* 2014). The long decay times we observed in motor areas cannot reflect the calcium indicator dynamics alone and suggest that sensory evidence triggers persistent responses in these regions.

We summarise the differences in response dynamic of cortical areas during ongoing decision-making in Figure 15. Both visual sensory and motor areas were strongly engaged by the stimulus, but with vastly different timecourses (Figure 16). Visual areas responded to stimulus with short latencies and short-lasting responses. On the other hand, frontal motor areas responses to the stimulus were persistent, with half-max latencies of secondary motor cortex following shortly after the response of visual sensory areas.

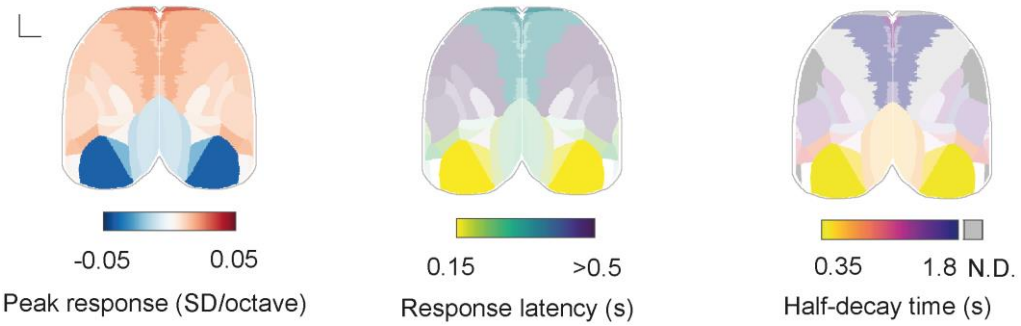

Figure 15. Subthreshold stimulus fluctuations trigger a localized cascade of activity across dorsal cortex. Left – Peak response across cortical areas. Middle – response latency (time to half maximum) across cortical areas. Shading based on response magnitude (left). Right – response half-decay time across brain regions. Saturation is scaled based on response magnitude (left). Regions for which half-decay time could not be determined are shown in grey (half-decay times longer than 4s).

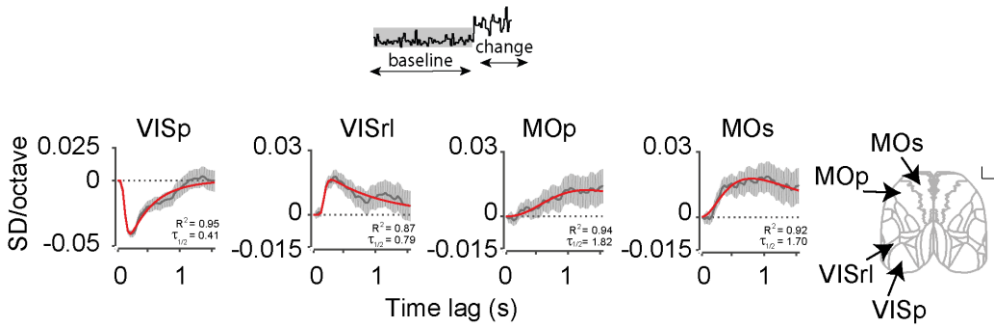

Figure 16. Different timecourses of stimulus responses between sensory and motor cortical areas. regression coefficients of widefield fluorescence against baseline stimulus TF across time, in selected ROIs on sensory-motor axis; regression coefficients (grey, 95% CI) and multiexponential fit (red). Inset – shading indicates the analysed trial epoch.

4.2.2. Extremes of stimulus evoke different responses in dorsal cortex

The previous section describes the sign and the timecourse of modulation of dorsal cortex by the visual stimulus during decision-making. However, the exact details of this relationship cannot be revealed by this analysis. For example, while the analysis above indicates that MOs activity is positively correlated with the TF of the stimulus, we cannot discern if this is due to the activity of MOs decreasing when the TF of stimulus decreases or the activity of MOs increases when the TF of stimulus increases. To disambiguate between these two scenarios, we probed how the extremes of the stimulus modulated cortical activity. Fast stimulus samples carried pro-licking information for the animal - increase in speed suggests that the change has probably occurred. In contrast, slow samples carried anti-licking information – decrease in speed suggests the change is not likely. We compared the influence of fast (1.5 standard deviations above the mean TF, N = 41194) and slow (1.5 standard deviations bellow the mean TF, N = 42253) samples during the baseline period, relative to responses near the mean TF (+/- 0.5 standard deviations, N = 467681 pulses) (Figure 17). We found that the anterior motor portion of the cortex responded to fast pulses selectively with an increase in activity. Importantly, the difference in responses to fast and slow samples could not be explained by differences in overt movement (Figure 18B). In contrast, visual sensory areas VISp and VISpm responded to both stimulus extremes, with increases in activity to slow samples and decreases in activity to fast samples. The opposite relationship was true for anterior higher visual areas (Figure 17A, 18A). This is consistent with response properties of these areas to passive visual stimulation, where VISp and VISpm neurons tend to prefer slow speeds, and neurons in areas VISal, VISrl, and VISa preferentially respond to higher speeds (Andermann *et al.* 2011, Marshel *et al.* 2011). In naïve animals both fast and slow samples

modulated the activity of sensory areas but there was no engagement of anterior motor areas (Figure 17 B, 19).

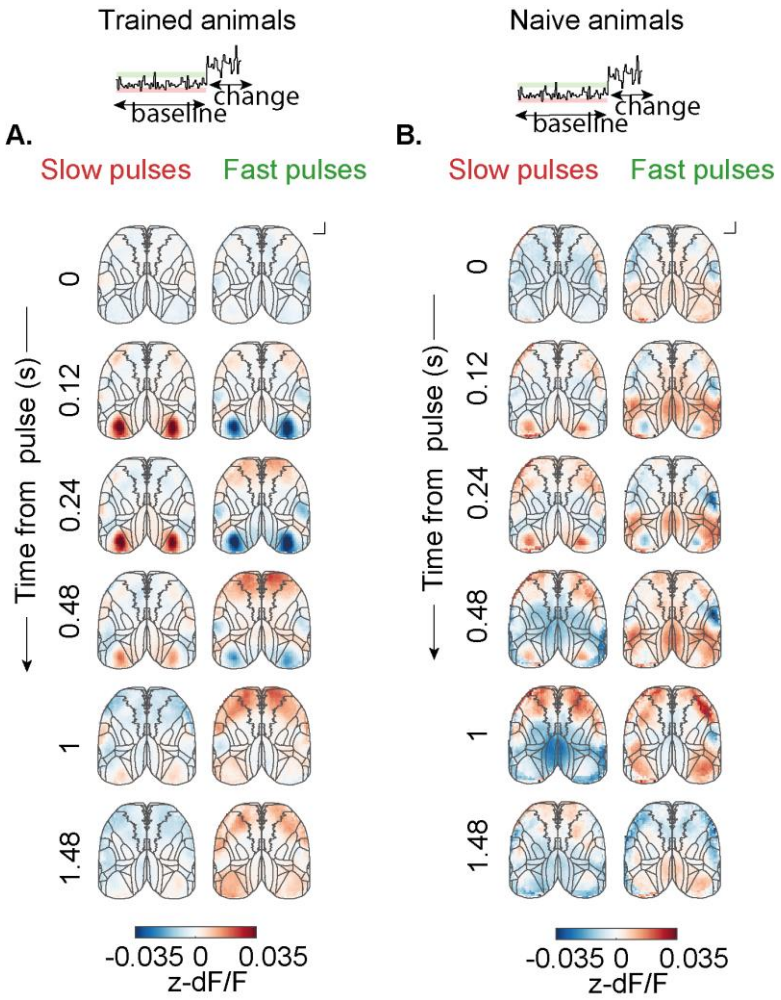

Figure 17. **Cortical responses to extremes of stimulus distributions in trained and naïve animals.** Maps of mean z-scored fluorescence responses to anti- (slow) and pro-licking (fast) subthreshold stimulus fluctuations in **A.** trained (6 mice) and **B.** naïve mice (3 mice) animals. Scale bar – 1 mm. Inset – shading indicates the analysed trial epoch.

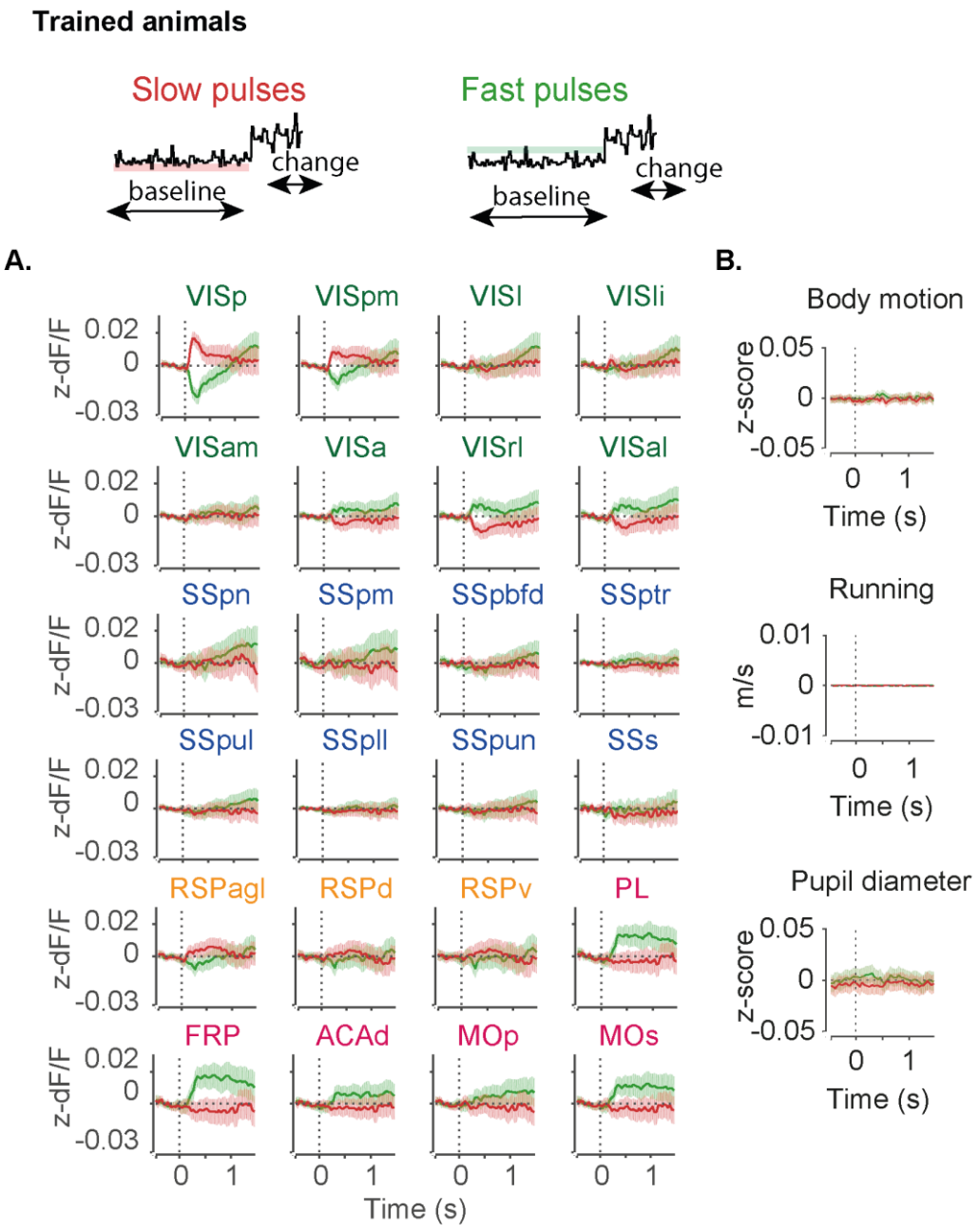

Figure 18. Timecourse of cortical responses to the extremes of the baseline stimulus distribution in trained animals. Mean z-scored fluorescence of imaged ROIs **A.** and behavioural measures **B.** aligned to anti- (slow, red) and pro-licking (fast, green) subthreshold stimulus fluctuations. Shading is 95% CI. Inset – shading indicates the analysed trial epoch.

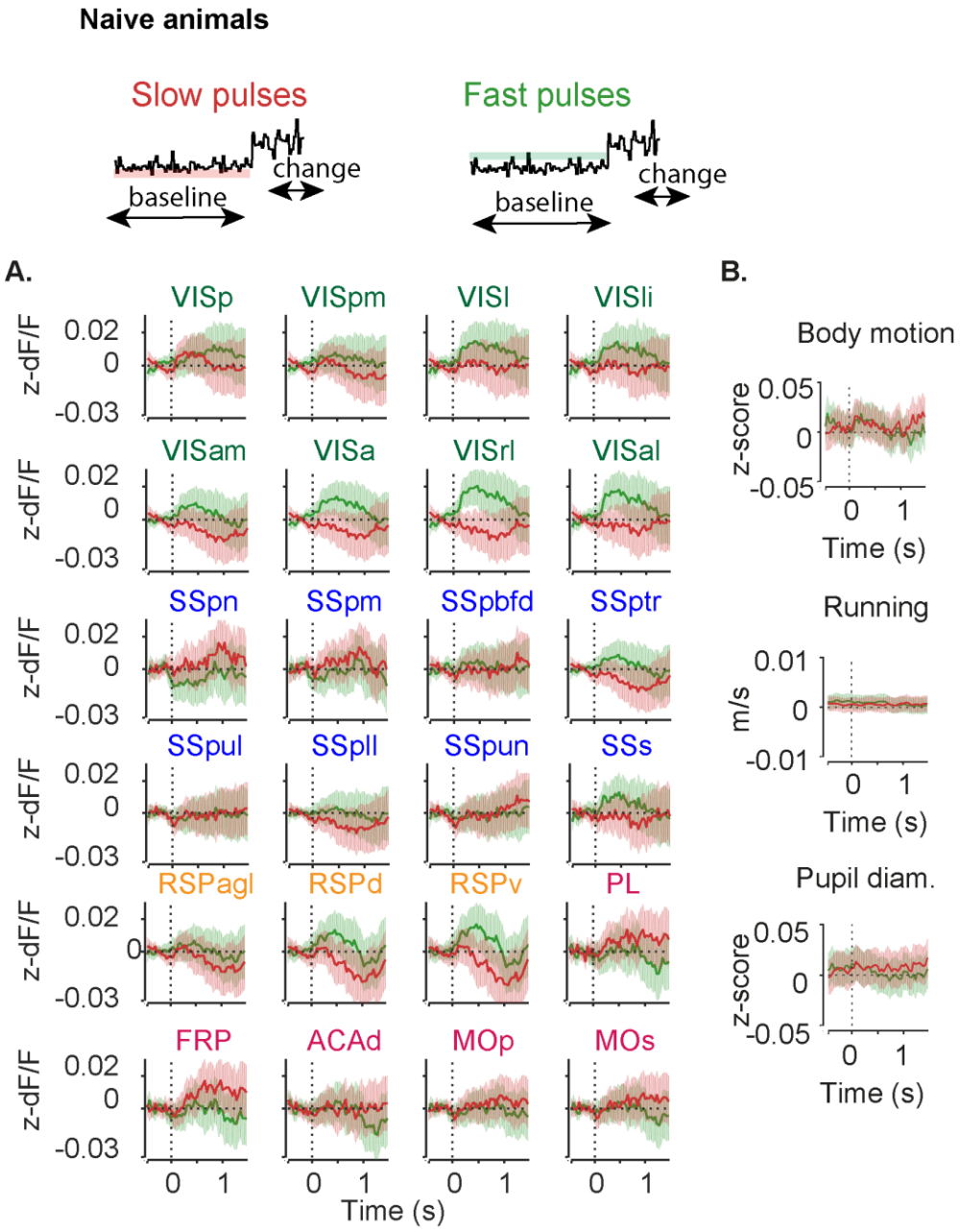

Figure 19. **Timecourse of cortical responses to the extremes of the baseline stimulus distributions in naïve animals.** Mean z-scored fluorescence of imaged ROIs **A.** and behavioural measures **B.** aligned to anti- (slow, red) and pro-licking (fast, green) subthreshold stimulus fluctuations. Shading is 95% CI. Inset – shading indicates the analysed trial epoch.

In summary, the extremes of the stimulus speed had differential effects on the activity of dorsal cortex in sensory and motor areas (Figure 20). Sensory areas responded to stimulus bidirectionally and motor areas responded selectively only to speed-ups in stimulus (larger TF). Motor cortex responses were selective for pro-lick relevant stimulus features (fast stimulus samples) and were sustained on long timescales after the presentation of the stimulus sample. In addition, primary and secondary motor areas differed in their onset dynamics. While primary motor cortex showed on average gradually increase in activity, the responses of secondary motor cortex were more abrupt. Such activity profile where representation of the relevant stimulus samples is strong and sustained can serve as signature of evidence accumulation.

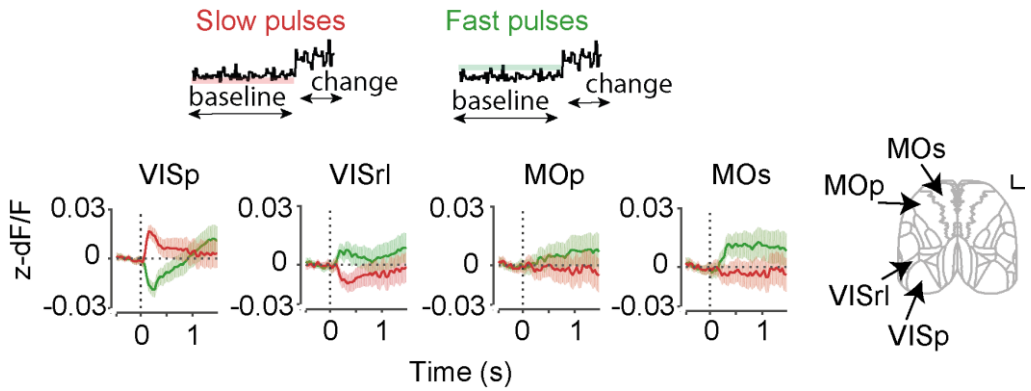

Figure 20. **Different timecourses of responses to the extremes of the baseline stimulus distribution between sensory and motor cortical areas.** Mean z-scored fluorescence aligned to anti- (slow, red) and pro-licking (fast, green) subthreshold stimulus fluctuations. Shading is 95% CI. Inset – shading indicates the analysed trial epoch.

4.3. Discussion

We found that stimulus evoked responses in the dorsal cortex depended both on past animals' experience and on the current stimulus content. While visual sensory areas responded to the full stimulus range in both trained and naïve animals, frontal areas were modulated by the speed of individual stimulus samples in trained mice only. Engagement of motor areas during learning has been previously described (Makino *et al.* 2017), but to our knowledge this is a first demonstration of engagement of motor areas over learning in the absence of overt motor output. Faster stimulus speeds that signal that the baseline speed has likely changed engaged both primary and secondary motor cortex, while slow stimulus samples that signal that the change has likely not happened yet did not recruit frontal motor areas. Specifically, secondary motor cortex responded to sensory evidence with short latencies after the visual sensory areas and is followed by recruitment of primary motor cortex. MOs is selectively modulated by incoming sensory evidence long after the disappearance of the relevant stimulus sample (> 1.5 s half-decay time) even in the absence of motor action. Therefore, two types of stimulus processing seem to be reflected in the activity of MOs during the deliberation period - filtering of sensory evidence for action-promoting stimulus samples, and maintenance of the history of past relevant stimulus samples. The filtering of sensory evidence may be learnt potentiation of direct projections from visual areas to the medial portion of secondary motor cortex (Zhang *et al.* 2016) or trough indirect pathway via the dorsomedial striatum (Khibnik *et al.* 2014, Hintiryan *et al.* 2016) and motor thalamus (Hooks *et al.* 2013, Guo *et al.* 2017, Winnubst *et al.* 2019). The modulation by relevant stimulus samples on prolonged timescales can also be supported by recurrent cortico-striatal-thalamo-cortical loop

involving the secondary motor cortex (Hooks *et al.* 2013, Winnubst *et al.* 2019) as shown in working memory tasks (Guo *et al.* 2017). Since widefield calcium imaging measures local average of activity (Makino *et al.* 2017), we are unable to discern whether the sustained activity in secondary motor cortex is carried by one homogeneous population, or if it is mediated by separate populations with different timecourses of activity (Harvey et al., 2012; Scott et al., 2017).Secondary motor cortex is thought to exert control over motor action by directly targeting the deep layer output neurons in primary motor cortex that project to the brainstem and spinal cord (Hooks et al., 2013). The latencies of responses in our task support this hierarchy between motor areas. Anatomical studies and physiological evidence from our data and others support the possibility that secondary motor cortex could serve as a hub between incoming sensory evidence and motor action (Barthas and Kwan 2017, Ebbesen *et al.* 2018). Pre-movement activity in frontal cortex is thought to reflect and control the state of a dynamical system that produces movement (Churchland *et al.* 2010, Shenoy *et al.* 2013, Kaufman *et al.* 2014, Murakami and Mainen 2015). We cannot discern processes of motor preparation from processes of decision-making and future task versions can be developed to answer this question, but whether these processes indeed involve different brain circuits remains controversial (Gold and Shadlen 2000, Bennur and Gold 2011, Svoboda and Li 2018). However, the activity we observed during decision-making in the baseline period differed from global choice-execution related activity - as described by us (Chapter 5) and others (Allen *et al.* 2017, Steinmetz *et al.* 2018, Musall *et al.* 2019), suggesting we were able to disambiguate the related and often concurrent processes of decision-making and choice execution.

Chapter 5. Neural responses during choice execution and other overt behaviour

5.1. Lick-related signals are represented globally across the dorsal cortex

We next examined the pattern of activity evoked by changes in the mean TF of the grating that the mice were trained to detect. On hit trials, change onset was followed by an increase in fluorescence across the dorsal surface of the cortex (Figure 21, 1974 noisy trials).

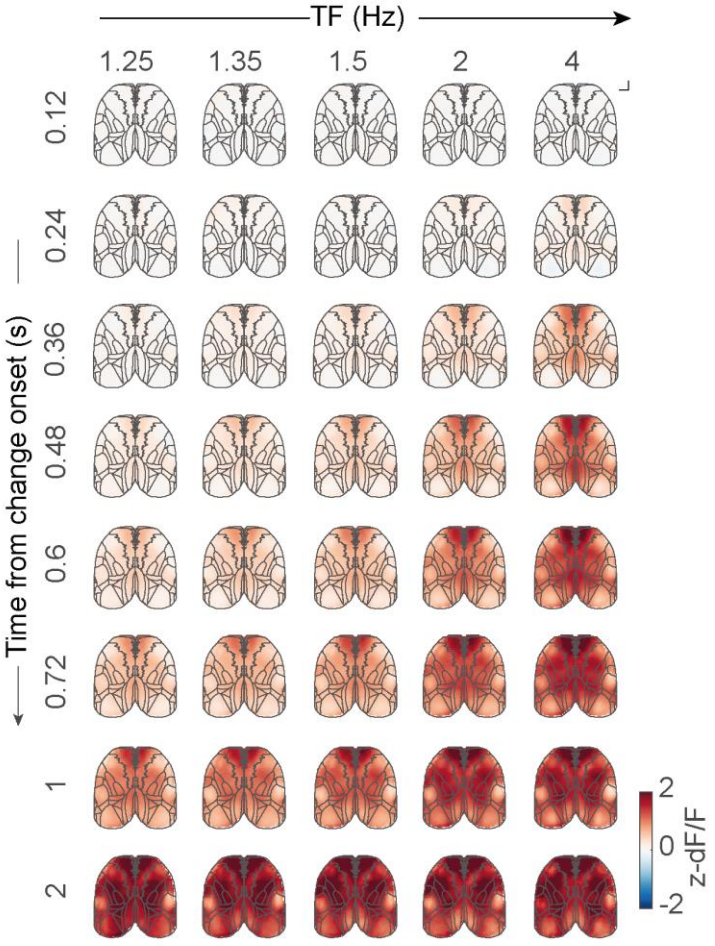

Figure 21. **Responses across the dorsal cortex during the change period.** Maps of mean z-scored fluorescence across the dorsal cortex aligned to change onsets on hit trials sorted by change strength. Scale bar – 1 mm.

The latencies of neural responses decreased as the strength of change increased (Figure 22), as it was the case with animals' reaction times (Figure 3B).

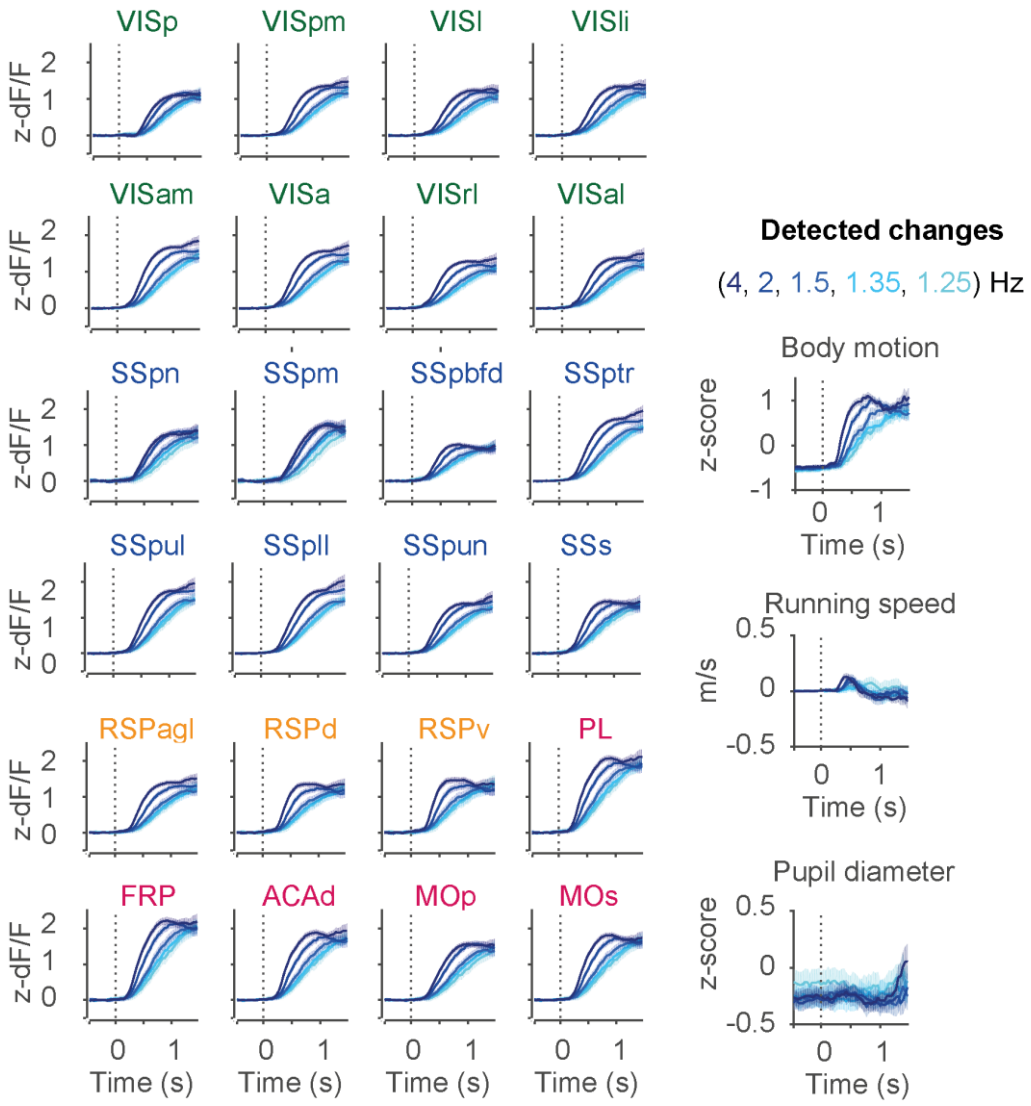

Figure 22. Timecourse of responses across the dorsal cortex during the change period. Mean z-scored fluorescence of imaged ROIs and behavioural measures (inset) across change strengths aligned to change onsets (dashed line) on hit trials. Shading is 95% CI.

However, several lines of evidence suggest that these responses primarily relate to the execution of choice rather than sensory components of the task leading up to it. First, these responses occurred earliest in motor areas, with latency of ~480 ms after change onset for the strongest stimuli (secondary motor area – MOs; time to half-max response) compared to ~600 ms latency for primary visual cortex – VISp (Figure 23), while for more difficult trials response latencies followed the increase in reaction times. Second, across stimulus strengths, the timecourse of responses followed the movement of the mouse, as captured by the body camera (Figure 22, body motion). Third, this global modulation of cortical activity was not observed on miss trials (Figure 24, 463 noisy trials).

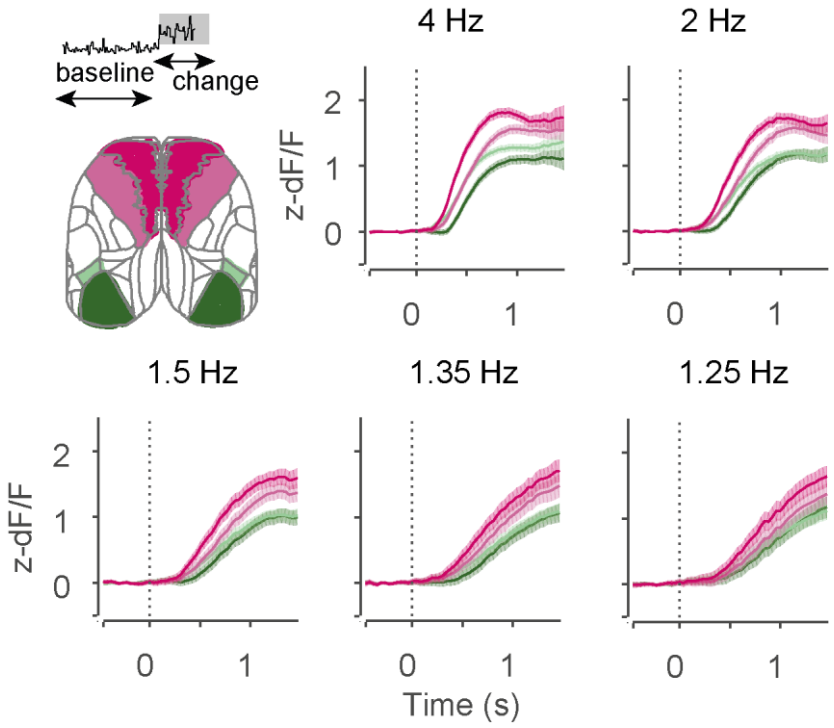

Figure 23. Timecourse of change onset responses on hit trials across the change strengths. Mean z-scored fluorescence of selected ROIs and across change strengths aligned to change onsets on hit trials. Shading is 95% CI. Inset – shading indicates the analysed trial epoch.

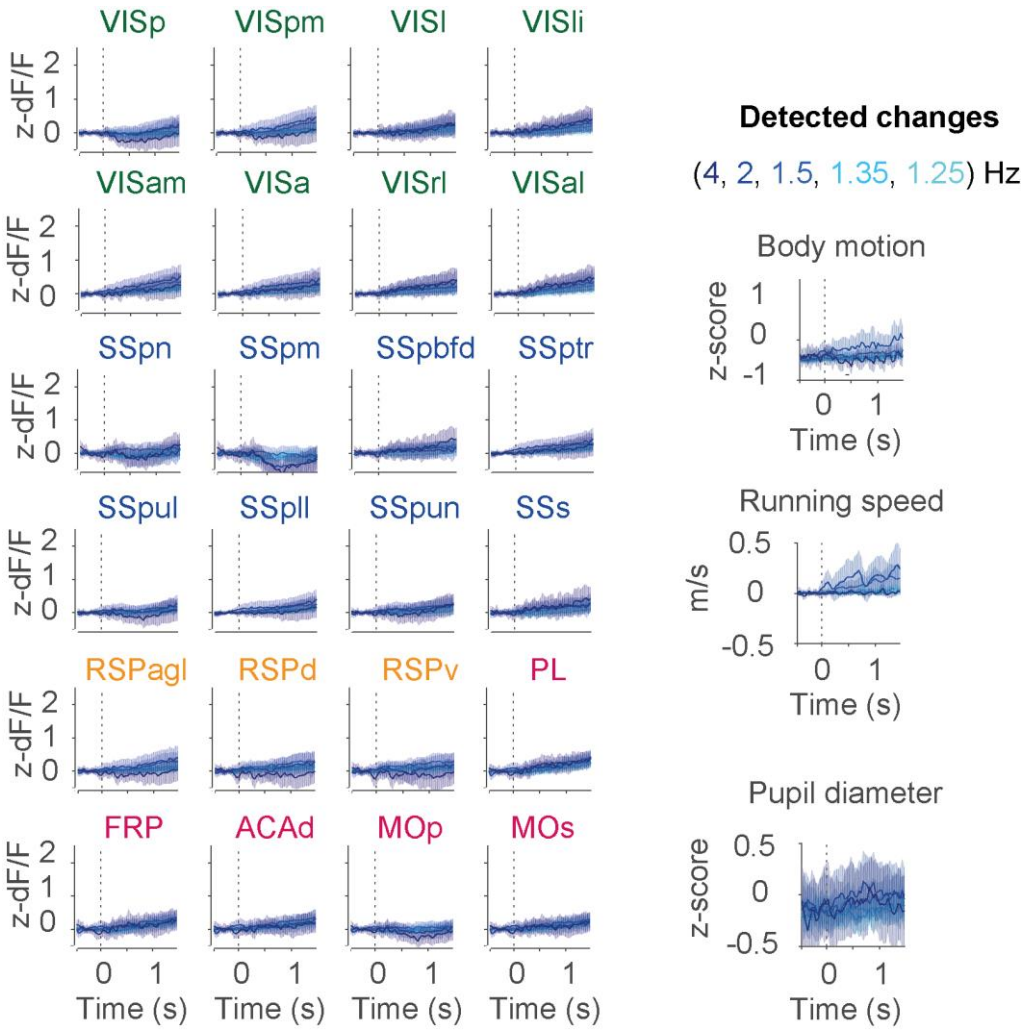

Figure 24. **Timecourse of responses across the dorsal cortex during the change period in miss trials.** Mean z-scored fluorescence of imaged ROIs and behavioural measures (inset on the right) across change strengths aligned to change onsets (dashed line) on miss trials. Shading is 95% CI.

Finally, same fluorescence responses once aligned to licks after the change across the stimulus strengths (Figure 25, 26) and during the baseline period (Figure 25, 27, 1564 noisy trials) became were stereotyped, without clear relationship with the stimulus strengths.

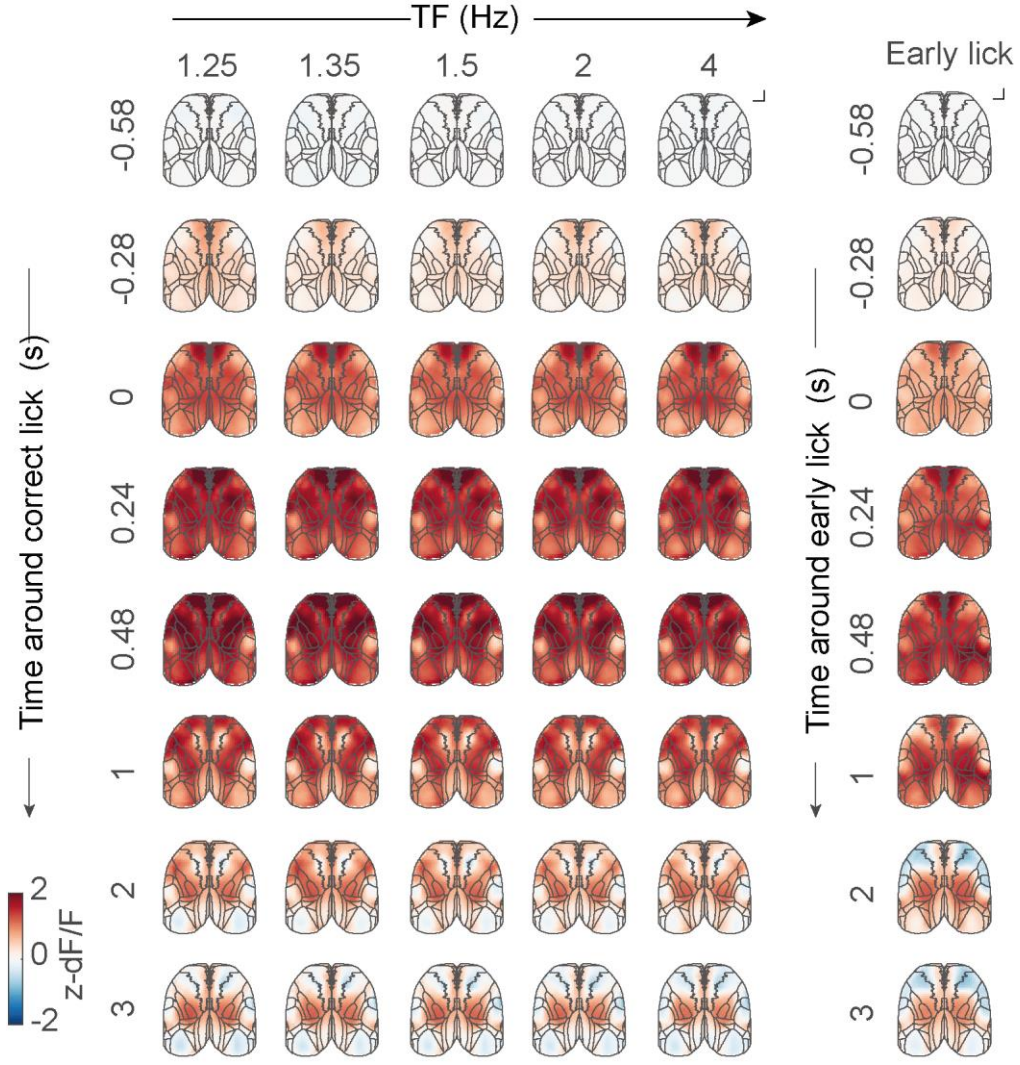

Figure 25. **Responses across dorsal cortex during licking.** Maps of mean z-scored fluorescence across the dorsal cortex aligned to lick onsets on hit trials sorted by change strength (left) and early licks (right). Scale bar – 1 mm.

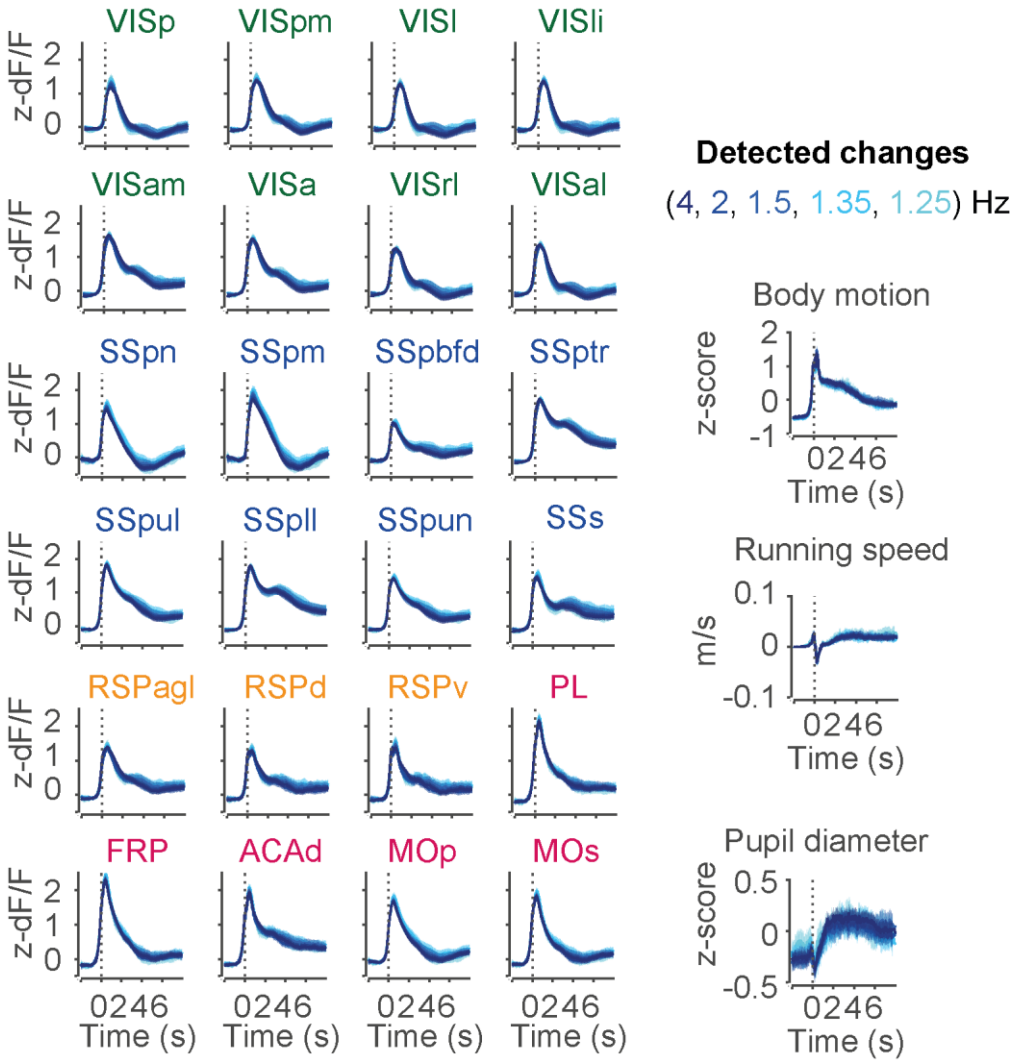

Figure 26. Timecourse of responses across the dorsal cortex during correct licks. Mean z-scored fluorescence of imaged ROIs and behavioural measures (inset on the right) across change strengths aligned to correct lick onsets (hit licks). Shading is 95% CI.

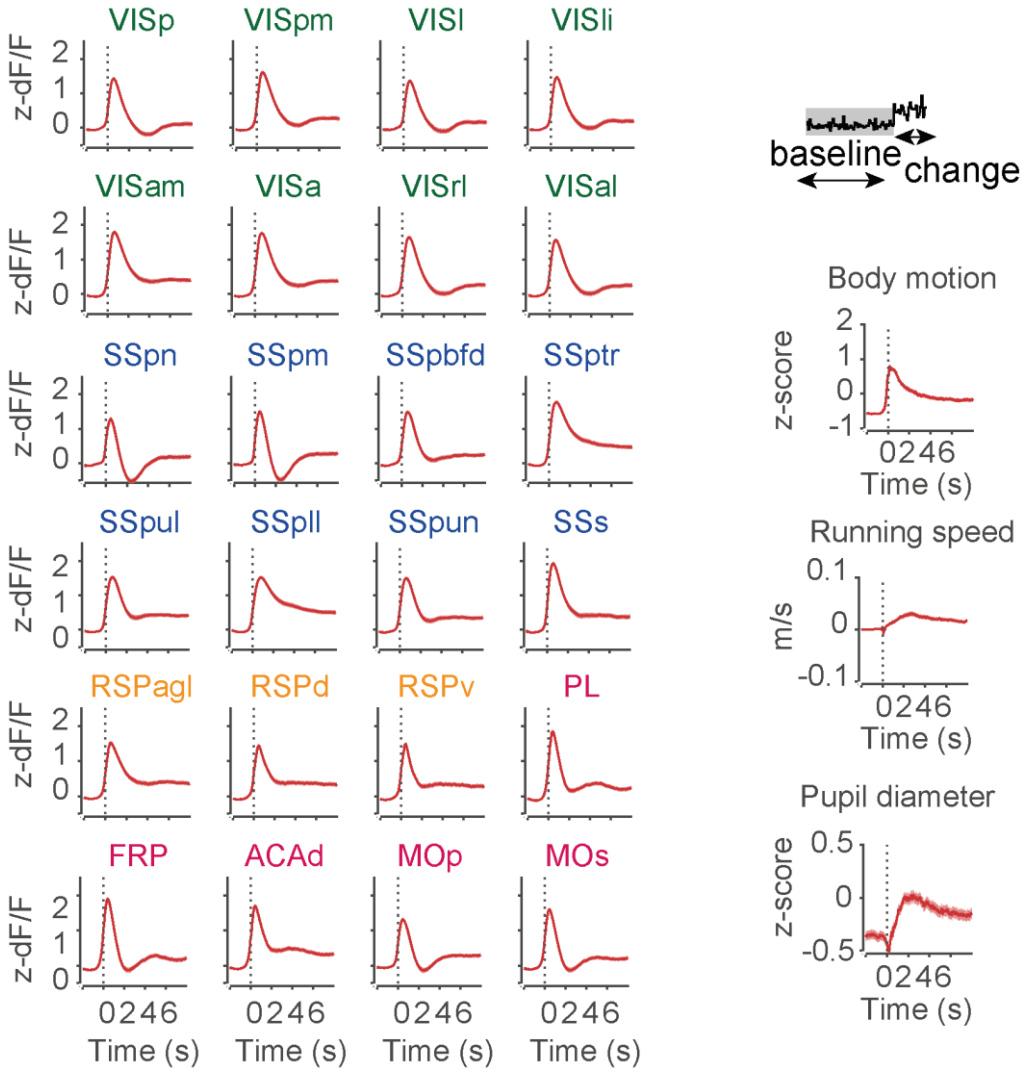

Figure 27. Timecourse of responses across the dorsal cortex during early licks. Mean z-scored fluorescence of imaged ROIs and behavioural measures (inset, shading indicates the analysed trial epoch) across change strengths aligned to early lick onsets. Shading is 95% CI.

Lick-related activity appeared earliest in secondary motor cortex, anterior visual and midline areas (VISal 360 ms prior to lick; VISam, VISa, VISrl, MOs, RSPd, ACAd 320 ms; quantified as the time to cross 10% of maximum response on 1.5 Hz change trials), followed by primary motor cortex, somatosensory cortex, and primary visual cortex (SSptr 280 ms; MOp, SSpul, SSpll, 240 ms; VISp, SSpn 200 ms; SSpm 160 ms; Figure 28A).

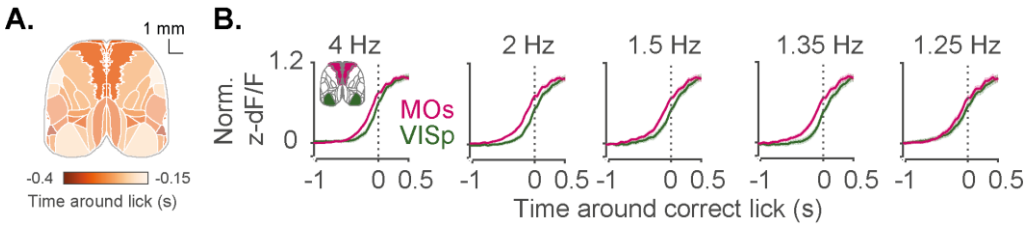

Figure 28. Cortical responses preceding the lick. A. Time to cross 10% of maximum response on 1.5 Hz change trials. **B.** Pre-lick activity of secondary motor cortex precedes activity in primary visual cortex (normalized to peak activity for each ROI).

Therefore, the apparent relationship between the stimulus strength and the activity of areas in the dorsal cortex (Figure 21-22) seems to be indirect. The choice execution related signals evolved at different rates from the onset of the change since animals responded faster to stronger stimuli and slower to weaker stimuli, as indicated by lick detection and onsets of body motion (Figure 29 – top). Controlling for this by aligning to onset of licking (Figure 29 - bottom) eliminated the relationship between cortical activity and the change strength.

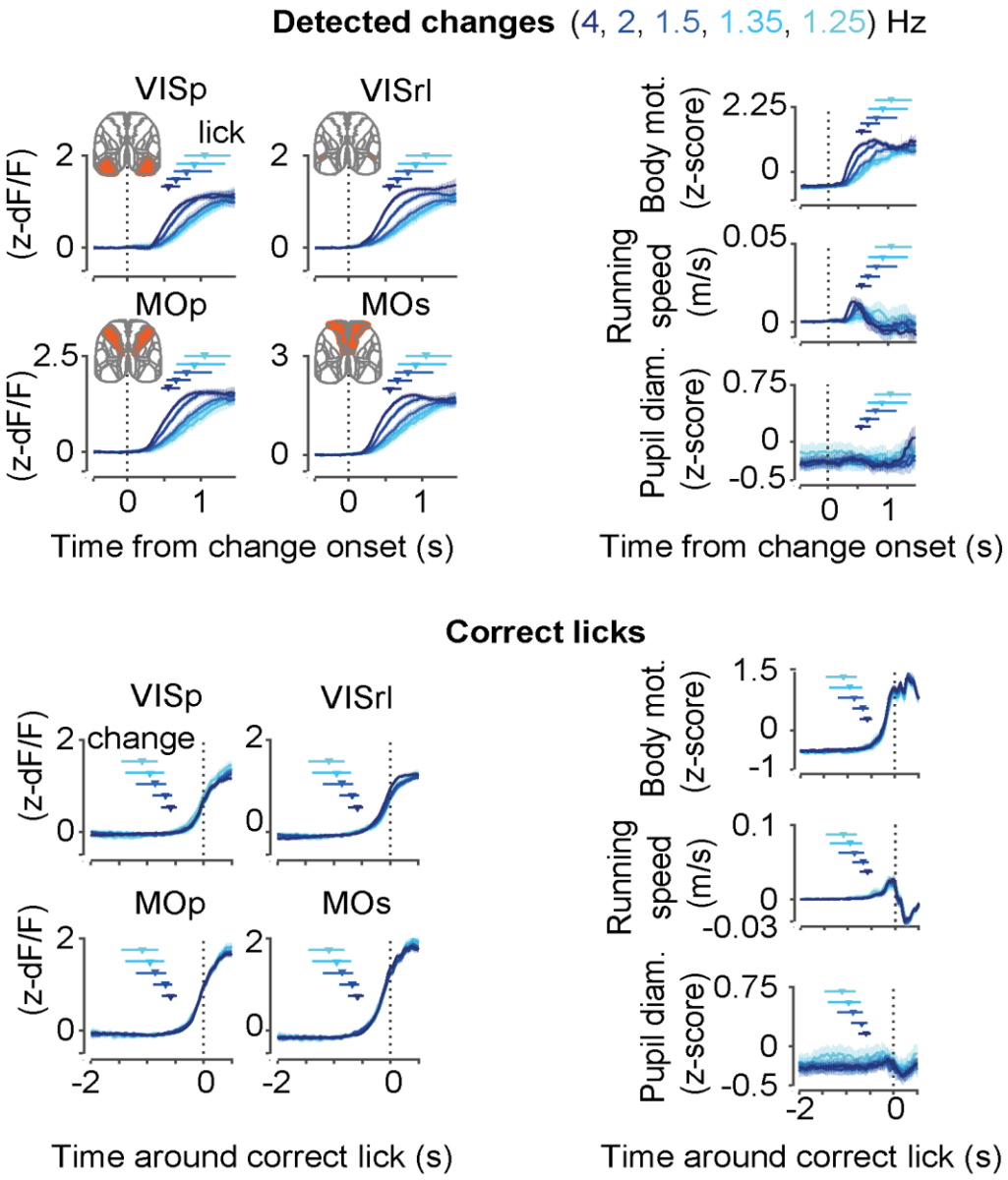

Figure 29. Responses across the dorsal cortex during the change period are global and dominated by licking-related activity. Mean z-scored fluorescence of selected ROIs and behavioural measures across change strengths aligned to change onsets on hit trials (top) and aligned to correct lick onsets (bottom**).** Shading is 95% CI. Horizontal lines and markers represent the interquartile range and the median reaction times (top) or stimulus change times (bottom).

Aiming to characterize cortical activity leading up to animals' choices following change onset in absence of overt movement, we focused our analysis on trials with long reaction times (> 840 ms before the lick) (Figure 30). However, change onset triggered an increase in animals' body motion prior to licking in these trials as well.

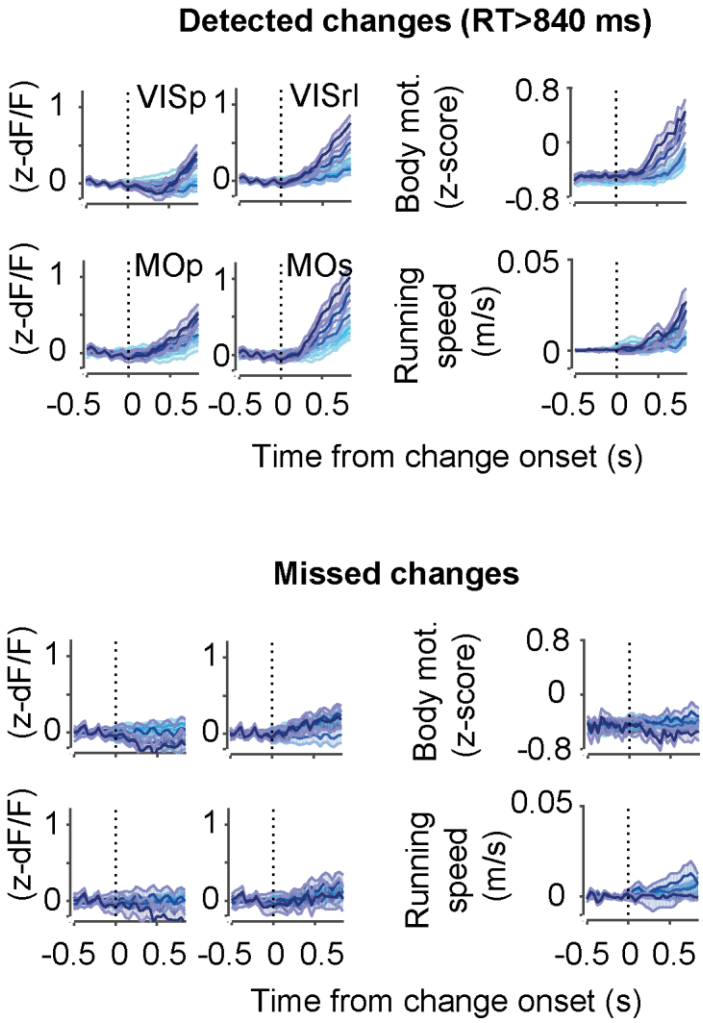

Figure 30. Responses across the dorsal cortex during the change period in long reaction time trials. Mean z-scored fluorescence of selected ROIs and behavioural measures across change strengths aligned to change onsets on hit trials where lick happened at least 840 ms from the change point (top) and miss trials (bottom). Body movements preceding licks accompany increase in activity on hit trials.

Together, these analyses strongly suggest that the global activation of the dorsal cortex following the change is associated with execution of the behavioural choice after the animal has committed to lick, and not with preparation of the choice that is dependent on the sensory component of the task.

5.2. Running modulates cortical activity profile during all epoch of the task

In the analyses described above we took care to minimize the impact of movement-related activity on our estimates of neural responses. In another version of the task, mice were required to run on the wheel to initiate a trial but were free to modulate their running speed during stimulus presentation. Performance of mice during running sessions was at the same level as in the stationary task (Figure 31, 82005 trials, 281 sessions, 6 mice). In this task mice were faster to respond, and the response window lasted 1.15s compared to 2.15s for stationary mice. Reaction time distributions followed the change strength as in the stationary version of the task (Figure 31B-C).

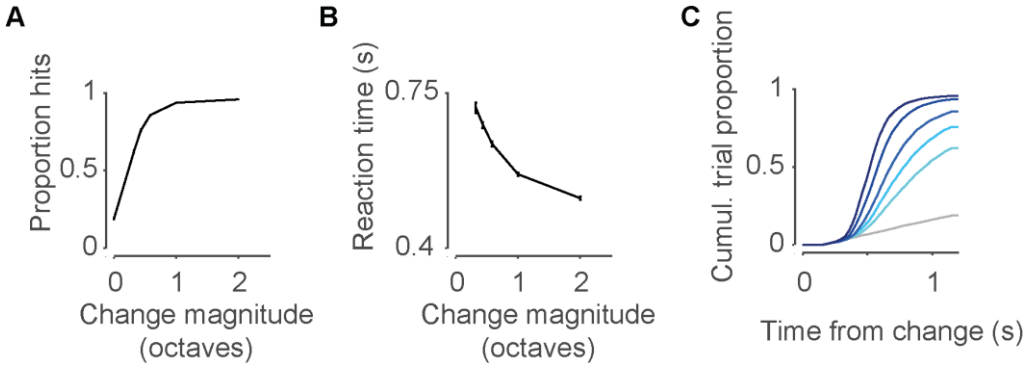

Figure 31. Performance of animals in the running version of the task. A. Detection rate and **B.** median reaction times are modulated by change magnitude (6 mice, error bars are 95% CI). **C.** Distribution of reaction times across stimulus changes Colours same as in Figure 3.

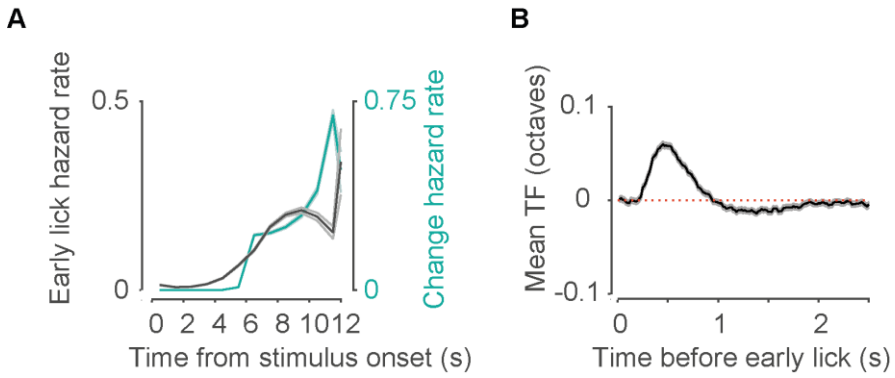

Figure 32. **Animal behaviour during baseline period. A.** Early lick hazard rate (grey) and change hazard rate (cyan). **B.** Average stimulus TF preceding licks during the baseline stimulus (6 mice, shading is 95% CI).

Change times were drawn from a single distribution, but as in the stationary task, mice did not lick randomly during the baseline period, but the early lick hazard rate reflected the change hazard rate (Figure 32A). Psychophysical reverse correlation revealed that as in the stationary mice, mice behaviour in the running version of the task was modulated by stimulus fluctuations over ~1 second (Figure 32B).

Although this was not explicitly encouraged by the task, we found that mice changed their running speed in response to the baseline grating stimulus – increasing their speed on average after slow stimulus samples, and decreasing their speed after fast stimulus samples (Figure 33 - top). The resulting correlation between baseline stimulus TF and running speed confounded the interpretation of widefield fluorescence responses. In contrast to the localized cascade of activity we observed in stationary mice, baseline stimulus fluctuations in running mice were followed by global modulation of dorsal cortical activity (Figure 33 - bottom; stationary - fast samples: N = 41194 frames, slow samples: 42253 frames, 6894 trials, 47 sessions, 6 mice) running - fast samples: N = 42004 frames, slow samples: 42870 frames, reference samples: 481756, 5930 trials, 37 sessions, 6 mice).

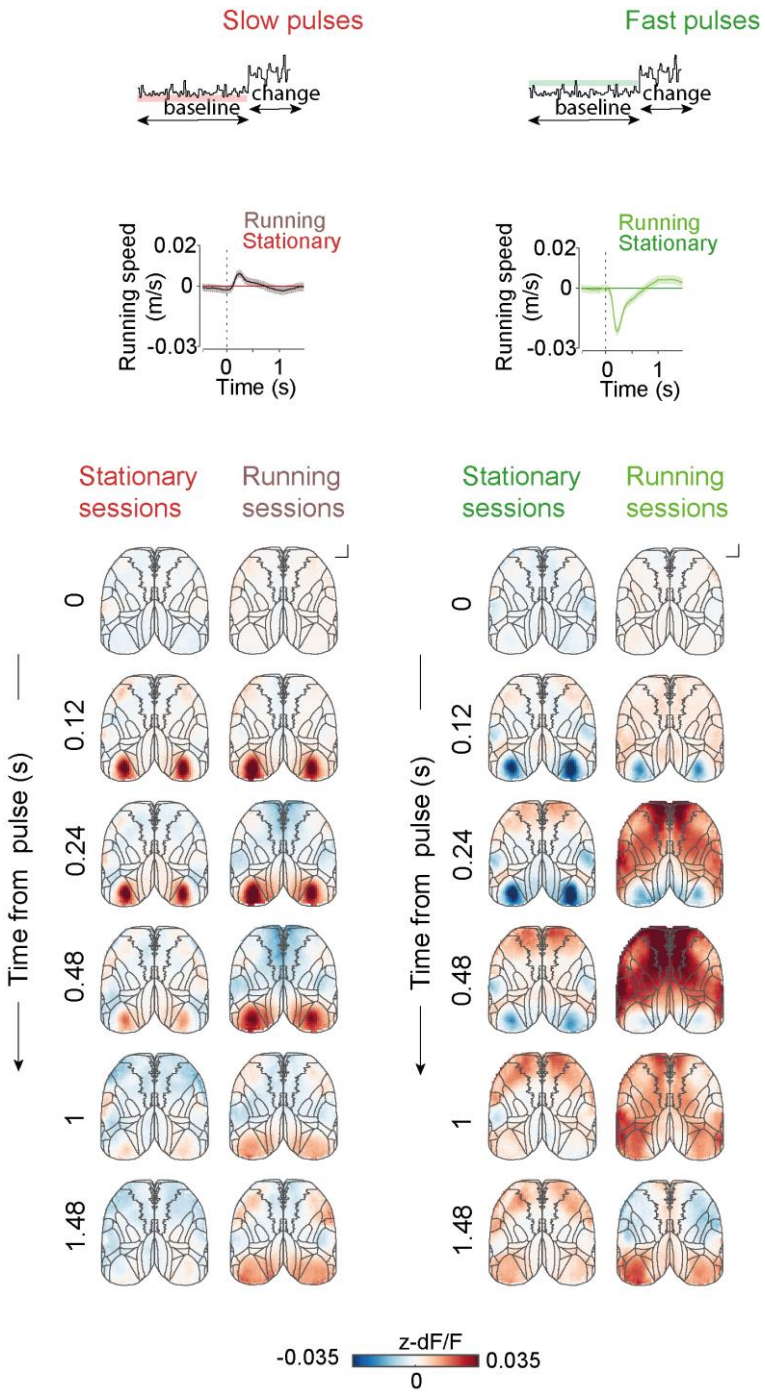

Figure 33. Cortical responses to extremes of stimulus distributions in stationary and running animals. Top – left: slow pulses in running but not stationary mice are followed by an increase in running speed. Top – right: fast pulses in running but not stationary mice are followed by a reduction in running speed. Bottom: Maps of mean z-scored fluorescence responses to anti-licking (slow pulses, left) and pro-licking (fast pulses, right) subthreshold stimulus fluctuations during sessions when mice were required to remain stationary or free to run. Scale bar – 1 mm. Inset – shading indicates the analysed trial epoch.

The timecourse of these global responses resembled that of change in running behaviour but was opposite in sign (Figure 33, 34 and 35). Nevertheless, the strongest responses were observed in frontal cortex.

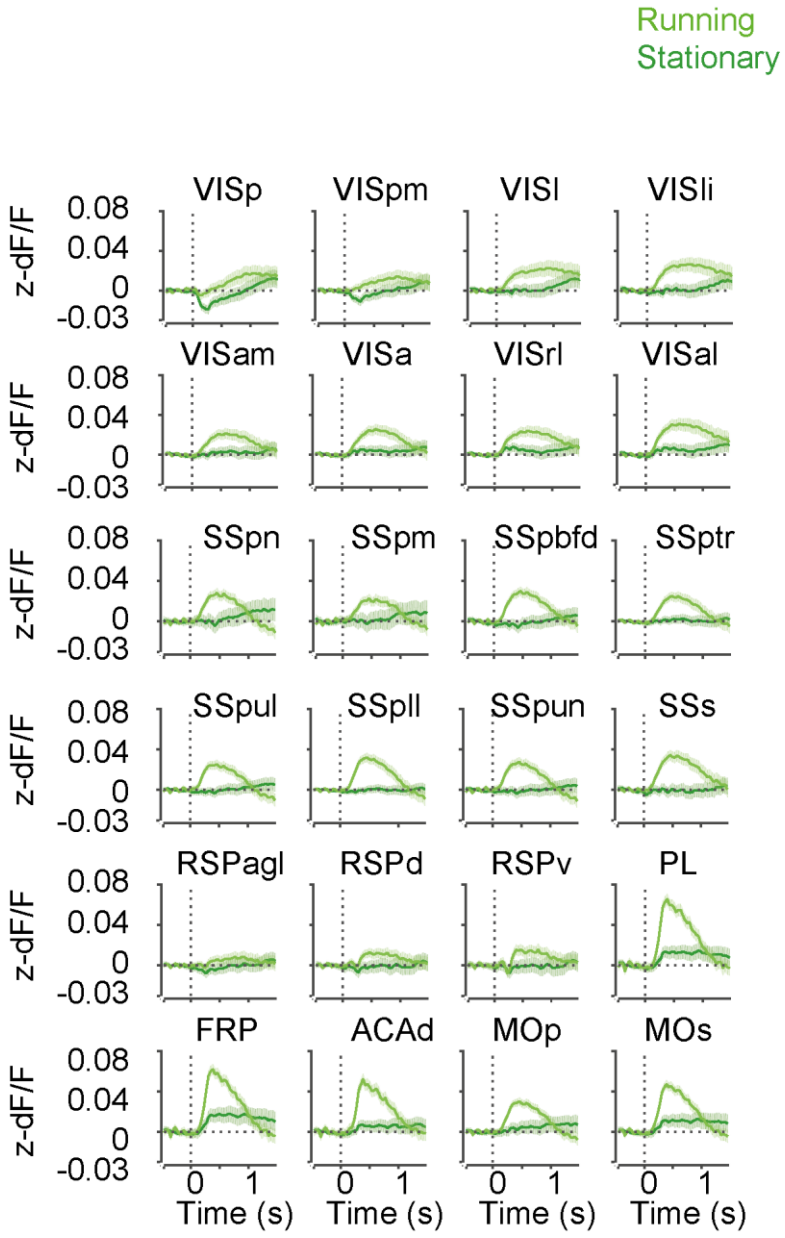

Figure 34. Timecourse of responses to fast pulses during running and stationary sessions across imaged ROIs. Mean z-scored fluorescence of all imaged ROIs aligned to pro-licking (fast) subthreshold stimulus fluctuations during sessions when mice were required to remain stationary (dark green) or free to run on the wheel (light green).

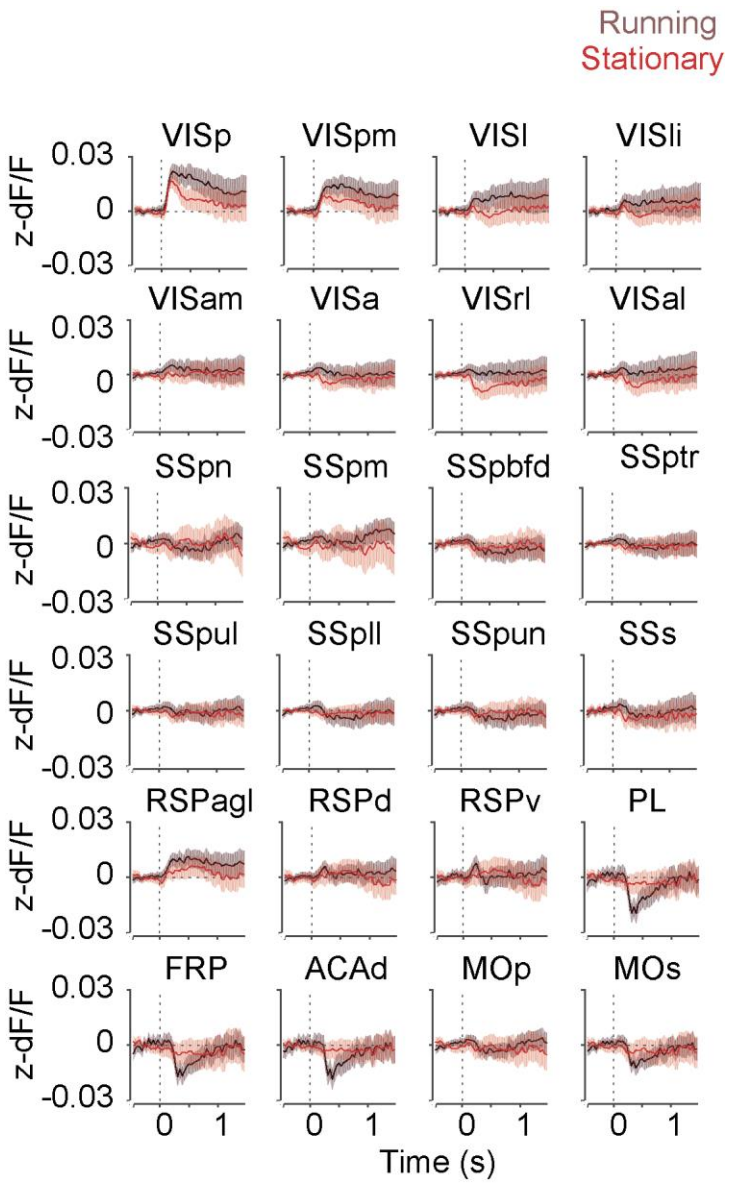

Figure 35. Timecourse of responses to slow pulses during running and stationary sessions across imaged ROIs. Mean z-scored fluorescence of all imaged ROIs aligned to pro-licking (fast) subthreshold stimulus fluctuations during sessions when mice were required to remain stationary (red) or free to run on the wheel (black).

These observations highlight the importance of controlling for movement in the interpretation of neural data and motivated us to focus our analyses on the stationary version of the task.

5.3. Discussion

Simultaneous recordings from multiple brain areas in work of others and the present study have demonstrated that task instructed and task non-instructed (spontaneous) motor output dominate brain activity (Allen *et al.* 2017, Steinmetz *et al.* 2018, Musall *et al.* 2019, Stringer *et al.* 2019). The question arises as to why does the brain have such strong and widespread movement signals? The nature of these signals is unknown, but their large scale and magnitude suggest that these signals play an important and general role in neural computations. These signals could reflect movement induced sensory input – reafference. Alternatively, this activity may be a consequence of the corollary discharge encoding an internal copy of the movement command. Such signals are found across the animal kingdom and are proposed to help locomoting animals distinguish between external and self-generated sensory inputs in order to correctly perceive the world around them (reviewed by Crapse and Sommer, 2008).

What is the mechanism of modulation of neural responses by movement? This question has been extensively studied in the visual cortex. It is proposed that the motor output acts as a gain on the visual responses as a part of locomotion related shift in the cortical state (Niell and Stryker 2010, Dadarlat and Stryker 2017). This gain mechanism is thought to be mediated by the basal forebrain (Fu *et al.* 2014) and inhibitory circuits in primary visual cortex (Garcia Del Molino *et al.* 2017, Dipoppa *et al.* 2018). In a specific case of visual–motor interactions, the function of these motor related signals is believed to be necessary to predict visual flow based on the motor output (Keller *et al.* 2012). The relationship between the movement and sensory input is established during the sensory experience and is incorporated into an internal model of the world.

In case when the expected and the experienced visual inputs do not match, an error signal is generated (Keller *et al.* 2012, Fiser *et al.* 2016, Heindorf *et al.* 2018) resulting from the difference between the excitatory drive from the motor-related prediction and the inhibition from the visual input (Attinger *et al.* 2017). The motor related prediction of visual flow is believed to be mediated by top-down projections from secondary motor and anterior cingulate cortex (Leinweber *et al.* 2017). Outside of the visual cortex, the efference copy of action, a specific case of corollary discharge, is believed to have wider role in reinforcement learning. Strong movement signals we observed in the cortex could serve as the substrate for associating appropriate actions with reward (Fee 2014).

How do these global movement related events impact the interpretation of awake behaving recordings? In the version of the task where animals could run, their running tended to correlate with the stimulus content - the animals slowed down after the presentation of a fast stimulus sample and sped up after the presentation of a slow stimulus sample. The change in animal running behaviour was driven by a cognitive process that considered the incoming sensory evidence. However, strong modulation of neural activity related to the change in running behaviour prevented us from characterizing its neural basis in an unbiased matter. Alternative to the post-hoc unmixing of movement related from task related activity (Musall *et al.* 2019), we decided to separate the two experimentally due to the high correlation and response amplitudes of running and task parameters. Similar global responses occurring around the choice execution, in our case licking, have been observed to dominate cortical activity, and seem to engage both excitatory and inhibitory populations across the cortex (Allen *et al.* 2017). In our task design, the extended periods of time where animal had to observe sensory evidence gave us the opportunity to characterize the

ongoing sensory-motor transformations without the confounds resulting from movements associated with the execution of the choice, results described in Chapter 4 and Chapter 5.

Chapter 6. Temporal expectation and sensorimotor transformations in the dorsal cortex

6.1. Temporal expectation gates the activation of motor cortex by sensory evidence

When making decisions, animals combine current sensory evidence and their predictions based on past experiences. We set out to examine how the processing of sensory evidence in the dorsal cortex is influenced by animals' temporal expectation of the stimulus change.

We compared the relationship between stimulus fluctuations and the widefield signals in the periods where the animal was expecting a change to occur (`early change` blocks) to those when the change was not expected (`late change` blocks) using linear regression (Figure 33; 255117 imaging frames from 2522 trials in early block and 524645 imaging frames 4376 trials in late block) as previously described in Chapter 4. We focused on the first 6 seconds after the baseline stimulus onset, when there was a difference in the early lick hazard rate between the blocks (Figure 5C).

We found that the relationship between stimulus speed and fluorescence was modulated by animals' temporal expectation of stimulus speed change (Figure 36), with the starkest differences observed in frontal motor areas.

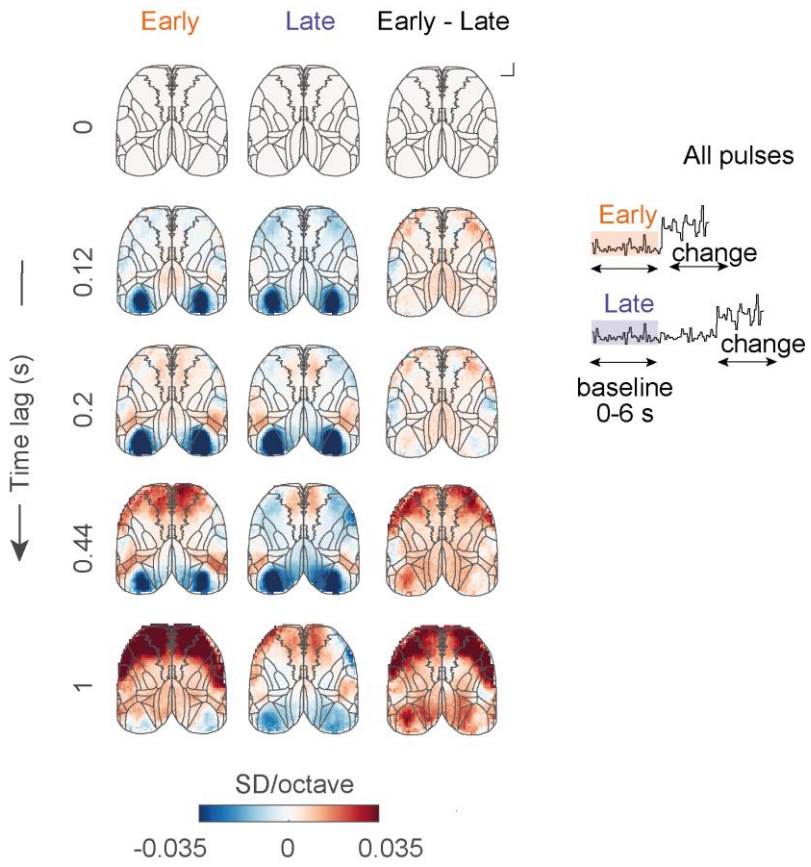

Figure 36. Temporal expectation modulates responses to stimulus fluctuations in motor areas. Regression coefficients of widefield fluorescence against baseline stimulus temporal frequency during 0-6 s of the trial in early (orange) and late (purple) change blocks, and difference between the blocks (early – late). Scale bar – 1 mm. Inset – shading indicates the analysed trial epoch.

Specifically, both secondary and primary motor cortices responded more strongly to stimulus fluctuations during the early blocks, when the changes were expected. In contrast, the initial responses to sensory evidence in visual areas were indistinguishable between early and late blocks and diverged in the later phase of the response (Figure 37).

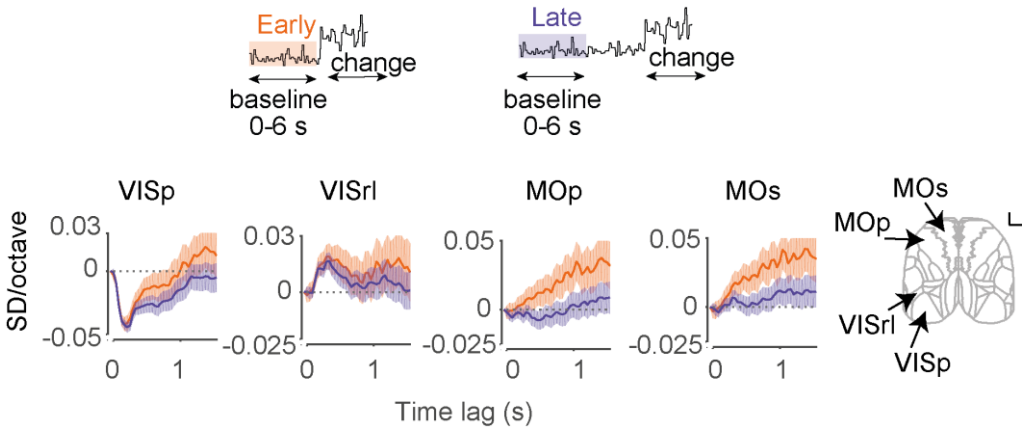

Figure 37. Different time course of temporal expectation modulation in sensory and motor cortical areas during baseline stimulus fluctuations. Shading is 95% CI. Inset – shading indicates the analysed trial epoch.

To understand how animals' temporal expectation affected processing of the sensory evidence in motor cortex, we computed mean responses to fast (pro-licking) and slow (anti-licking) stimulus pulses during the first 6 s of the trial in early and late change blocks (Figure 38; Early change block: fast pulses: N = 10105 imaging frames, slow pulses N = 10420 imaging frames, reference pulses: N = 114934 imaging frames. Late change block: fast pulses: N = 20997 imaging frames, slow pulses: N = 21224 imaging frames; reference pulses: N = 235576 imaging frames). Responses to slow stimulus pulses were similar between the two change blocks. On the other hand, responses to fast stimulus pulses in motor areas were enhanced when animals were expecting the change to occur (Figure 39). Thus, temporal expectation selectively enabled the transfer of task-relevant sensory information to secondary and primary motor cortex.

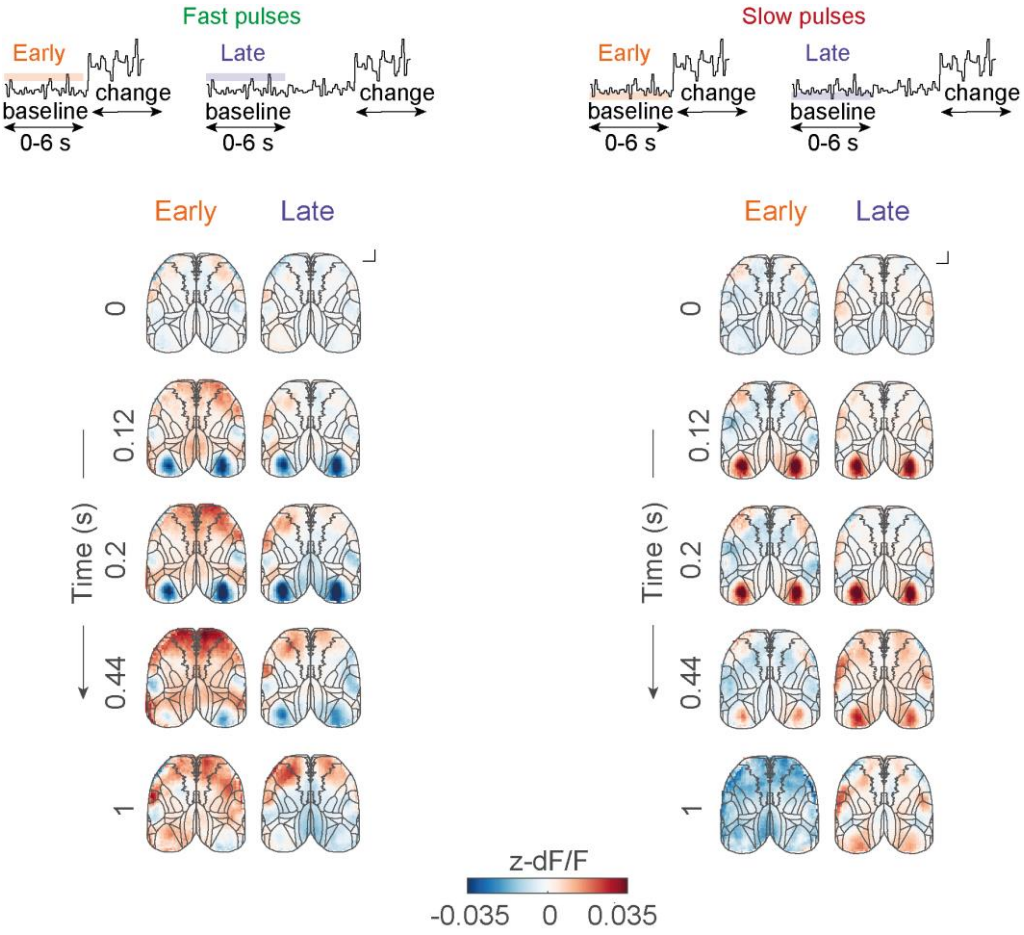

Figure 38. Cortical responses to extremes of the stimulus distribution across change blocks. Mean z-scored fluorescence responses to pro- (fast, left) and anti-licking (slow, right) subthreshold stimulus fluctuations during 0-6 s of the trial in early and late change blocks. Scale bar – 1 mm. Inset – shading indicates the analysed trial epoch.

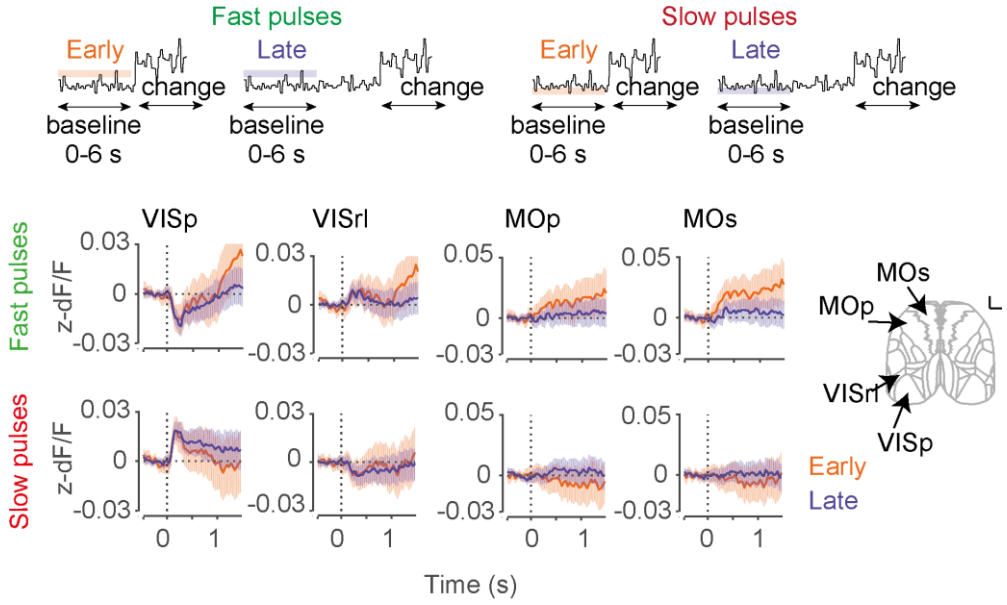

Figure 39. Timecourses of cortical responses to extremes of the stimulus distribution across change blocks between sensory and motor areas. Mean z-scored fluorescence responses to pro- (fast, top) and anti-licking (slow, bottom) subthreshold stimulus fluctuations during 0-6 s of the trial in early and late change blocks. Shading is 95% CI. Inset – shading indicates the analysed trial epoch.

6.2. Discussion

An important element in goal directed behaviour is not only choosing an appropriate action but also deciding when to act. We have observed modulation of primary and secondary motor cortex by temporal expectation that acted like a gate on incoming sensory evidence. Contrary to earlier studies in rodents (Jaramillo and Zador 2011) we did not observe expectation-related modulation in the average activity of sensory areas.

Basal ganglia and cerebellum have been implicated in self-timing tasks in primates, both contributing to different aspects of timing activity (Kunimatsu *et al.* 2018). Manipulation of dorsal striatum in a spatial visual change detection task resulted in a larger increase in reported changes when the change occurred on expected side (Wang *et al.* 2018). Similar gating might be mediated by the same structure in the domain of temporal expectation, especially as it has been demonstrated that the dorsal striatum receives projections from both frontal motor areas and visual areas (Khibnik *et al.* 2014, Hintiryan *et al.* 2016) and cortico-striatal projections from sensory cortex have been implicated in mediating influence of sensory evidence on perceptual decisions (Znamenskiy and Zador 2013). Given the proposed role of frontal regions in timing behaviour, the frontal cortex can provide both signals carrying relevant sensory information and relevant timing information to the dorsomedial striatum, that can act to promote the motor action by disinhibiting licking via the output structures of the basal ganglia.

Chapter 7. Conclusion and perspectives

We aimed to characterise the activity of the dorsal cortex during sensory-motor transformations that take place in perceptual decision making. To this end, we developed a new behavioural paradigm which enabled us to probe the responses of cortical areas to sensory evidence delivered in form of a parametrized stimulus to which the animals had to attend. Long trial duration allowed us to explore the effect of animals' expectation on this process.

We structured the trials such that the processes that were ongoing as the animal was making its decision were temporally well separated from the processes that were directly related to the execution of the choices that it made. We found that these engaged the dorsal cortex in profoundly different ways. Reporting of choice or execution of other overt movements triggered global and almost concurrent responses that dominated the activity of the dorsal cortex. On the other hand, ongoing sensory fluctuations during the deliberation period engaged the dorsal cortex in a defined spatio-temporal activity cascade involving only a subset of cortical areas. We found that primary and higher visual areas responded to stimulus fluctuations with low latencies and across the full stimulus range. On the other hand, responses in motor cortex occurred selectively following the pro-action (licking) stimulus only.

While the responses in primary motor cortex were slow, secondary motor cortex was modulated with short latencies following the activation of sensory areas and remained selectively influenced by the pro-action stimulus samples long after their presentation. These rapid and prolonged stimulus influences could serve as a substrate of sensory evidence accumulation or other strategies mice might use to solve the task. Furthermore, these influences of the pro-action stimulus were not static but were

dependent on past experiences and animals' expectation to when to act, boosted when the change was expected.

The proposed functional flow of sensory and movement-related signals in mouse dorsal cortex is depicted bellow (Figure 40).

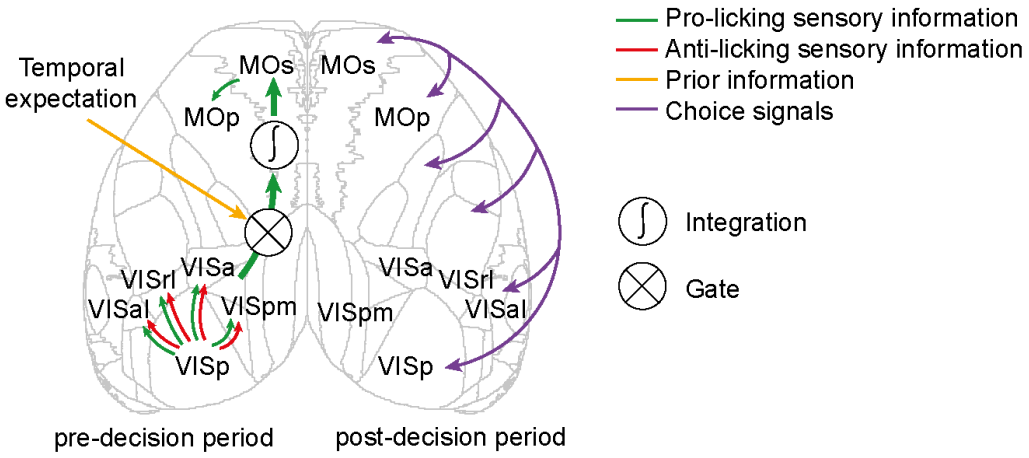

Figure 40. Proposed functional flow of sensory and movement-related signals during sensory-motor transformations in mouse dorsal cortex. Sensory information modulates activity in primary and higher visual areas. Only pro-licking sensory signals are transmitted to secondary motor cortex, where they persist on prolonged timescales. This functional flow from visual sensory areas to secondary motor cortex is gated by animals' expectation. When the animal executes its choice, movement-related preparation signals are broadcast globally across the dorsal cortex.

Although our results identify secondary motor cortex as an important hub for decision making in the dorsal cortex, in the present study we are unable to determine origins of these signals. Manipulation experiments and methods with better temporal

precision would enable us to determine whether the observed signals are mediated by cortico-cortical interactions or this specific and long-lasting modulation of secondary motor cortex is also supported by the basal ganglia, thalamic and/or cerebellar pathways.

Chapter 8. Methods

8.1. Animal subjects

All experiments were conducted in accordance with institutional animal welfare guidelines licensed by Swiss cantonal veterinary office. To express calcium indicator in excitatory cells throughout the cortex, we crossed heterozygous Camk2a-tTA (JAX#007004) and homozygous tetO-GCaMP6s (JAX#024742) mice (Wekselblatt *et al.* 2016).

8.2. Surgical procedures

Two weeks before the start of behavioural training, mice were switched to reversed light-cycle. Environment enrichment was provided in form of a running wheel and cardboard tunnels. After acclimatization, eleven adult male mice (84 – 104 days) underwent surgery to implant a head-plate and expose the skull over the dorsal cortex for transcranial imaging. Animals were anaesthetized with a mixture of fentanyl (0.05 mg per kg), midazolam (5.0 mg per kg), and medetomidine (0.5 mg per kg). The animal's skull was exposed and cleaned, and a metal head-plate was secured to the scull around the edge of the occipital plate and the superior temporal line using dental cement (Super-Bond C&B, Sun Medical). The exposed imaging site was covered with transparent dental cement (Polymer L-Type Clear, Sun Medical) and a glass coverslip (150 um thickness), pre-cut using a diamond scribe to match the exposed surface of

the skull (Silasi *et al.* 2016). A custom-made 3D printed light shield was then cemented to the preparation. For histology experiments mice were anaesthetized with sodium pentobarbital and transcardially perfused with 4% paraformaldehyde. The brains were extracted, post-fixed overnight in 4% paraformaldehyde, and stored in 50 mM phosphate buffer.

8.3. Details of the behavioural apparatus

Behavioural setup consisted of three main parts (i) head-fixation apparatus for the mouse, (ii) two monitors that delivered the visual stimulation on each side of the animal, (iii) custom electronic circuits that controlled reward delivery, delivery of air-puffs and amplified the licks that the animal made. Behavioural setups, similar as described in (Poort *et al.* 2015), were placed in sound isolated boxes. The mouse was head-fixed and placed on Styrofoam wheel (d = 20 cm, w = 12 cm). Wheel movements were monitored using a rotary encoder (pulse rate 1000, Kübler) coupled to the wheel axle. Two 21.5" monitors were placed on each side of the animal (~20 cm away from the animal, slightly angled and tilted towards animals' body), covering approximately 100x70 degrees of visual space. Monitors were gamma-corrected with maximum luminance of ~40 cd/m^2 (Konica Minolta, LS-100 Luminance Meter). Custom written software in MATLAB (MATLAB 2016b, The MathWorks) controlled stimulation using PsychToolbox-3 extension (Kleiner *et al.* 2007). Soy milk reward were delivered through the spout in front of the animal. Reward delivery was regulated via pinch valve (NResearch). The spout was coupled to a piezo element whose output was used to measure animals' licking. Custom electronic hardware was used to amplify

the piezo signals and control the valve. An air tube was placed ~3 cm from the animals' right cheek to deliver light air-puffs (200 ms, 2 bar pressure, tip was cut open to 2 mm). Animals' right eye was imaged with a CMOS camera (Imaging Source, 30 Hz) in order to tract eye movements and pupil diameter. A second camera was placed in front of the animal capturing animals' body movements. To increase throughput of animals, animals were trained in parallel on 5 different setups. Animals were assigned to the setups randomly from sessions to session. All non-neural data was acquired using custom written code in LabView (National Instruments) and PCI-6320 acquisition card (National Instruments).

8.4. Behavioural training

Before animals underwent training on the temporal frequency change detection task, several pre-training steps were taken in order to habituate the animal to the setup. One week after the surgery, mice were food-restricted and behavioural training started. Animals were handled for a minimum of 3 sessions, until mice were comfortable with the experimenter and were climbing on experimenters' hand while being given drops of soy milk. Animals were then introduced to short manual restraint periods in a soft cloth after which animal was given soy milk reward. Next, animals were head-fixed and placed on the running wheel of the behavioural training setup (10 – 20 min) with the monitors turned off and were trained to run on the wheel for reward. This step

typically took 4 sessions. Two mice were not trained further than this step and were assigned to the naïve cohort.

Next, to ensure that the animals understood the relationship between the stimulus presented on the monitor and reward availability, mice were pretrained on a simple task, where they had to lick in response to a change in the orientation of the grating. At this stage, translation of the grating was linked to the running speed of the mouse. As soon as mice started responding to the change in grating orientation, this step was complete. One mouse, which failed to learn to respond to orientation changes, was not trained further and was added to the naïve cohort. Eight mice proceeded training on the temporal frequency change detection task. Two of these mice were excluded from study due to lack of progress (too high abort rate due to early licks). It took the remaining six mice 14-21 sessions to learn the task. Mice were initially allowed to run during the task. After observing strong modulation of cortical activity associated with running, mice were required to be stationary during the task.

8.5. Details of the imaging setup

The macroscope consistent of two photographic lenses (85mm f/1.8D objective, 50mm f/1.4D tube lens, Nikon) that were placed in face-to-face orientation (Ratzlaff and Grinvald 1991). Excitation light from 470 nm (M470L3, Thorlabs, with excitation filter FF02-447/60-25, Semrock), and 405 nm LED (M405L3, Thorlabs, with excitation filter FF01-405/10-25, Semrock) was combined using a dichroic mirror (FF458-Di02-25x36, Semrock) and delivered in Koehler configuration through second dichroic mirror (FF495-Di03, Semrock). Images were acquired after emission

filter (525/50-25, Semrock) using an sCMOS camera (pco.edge 5.5, PCO) and provided manufacturers' software at 50 Hz in rolling shutter mode and binned on the fly 2x2.

8.6. Data analysis: pre-processing of imaging data

Saved frames were checked for dropped frames and XY motion artefacts and separated to 405 nm and 470 nm channels. The camera offset (average of 10000 dark frames) was removed from each frame. Each pixel in each session was low-cut filtered (cut-off at 0.00333 Hz), preserving the DC offset. Channel 405 nm was linearly interpolated to timepoints of 470 nm channel frames by taking the average 405 nm frames immediately before and after each 470 nm frame. Ratio of 470 and 405 channels was normalized by the mean of the ratio. To correct for differences in illumination and prep quality across the imaging site within individual sessions, and across sessions and animals, fluorescence traces for each pixel were normalized by their standard deviation within each imaging session.

8.7. Data analysis: behaviour

We included all the sessions after mice crossed the threshold of detecting more than 80% easiest changes in no-noise trials and interrupted less than 55% no-noise trials due to early licking. Average detection rate across sessions for easiest change was 96.9 ± 9.3% (mean ± sd), average early lick rate 19.36 ± 16.3%. We excluded

6/115 sessions due to high abort rate due to movement. In the remaining sessions average abort rate due to movement was 43.4 ± 17.8% where 52% of all movement induced aborts happened during the first 3.5 seconds of the stimulus).

When computing behavioural performance, all error bars are 95% confidence intervals, unless otherwise stated. For psychometric curves and hazard rates, confidence intervals were estimated using *binofit* in MATLAB, for chronometric curves they were calculated as the 0.025 and 0.975 quantiles of 2000 bootstrap samples with replacement).

To estimate hazard rates, the number of early licks and changes in one second bins was normalized by the total number of trials, excluding trials where early lick or change have already happened, or trial was aborted due to movement prior to the start of the bin.

To compute lick triggered averages, stimuli preceding early licks were averaged across animals, revealing mean stimulus information content prior to the lick. Confidence interval were estimated by resampling early licks (2000 bootstrap samples with replacement).

8.8. Data analysis: neural data

8.8.1. Responses to task events

To compute fluorescence responses associated with baseline stimulus onset, stimulus change, correct, and early licks, we first identified the imaging frame which was being exposed when a given event occurred. We then extracted fluorescence

traces around each event. For stimulus onset traces in Figures 11 and 12, we excluded frames acquired after change onset or less 1 second prior to early licks or wheel movement and resulting trials shorter than 0.5 s. Aligned traces were then baseline corrected by subtracting the mean fluorescence in 480 ms (for stimulus and change onset) or 2000 ms (for licks) prior to event onset.

8.8.2. Responses to subthreshold TF fluctuations

We first resampled the TF of the baseline stimulus at the sampling rate of the imaging acquisition. To do this, we computed the geometric mean TF presented during each imaging frame acquired during the baseline stimulus, weighted by their presentation duration:

$$\bar{\nu} = 2^q, \text{ where } q = \frac{\sum_{i=1}^{n} p_i \log_2 \nu_i}{\sum_{i=1}^{n} p_i}$$

ν_i is the TF of the i-th monitor frame presented during a given imaging frame, p_i is its duration (16.7 ms or less, for monitor frames, which spanned two imaging frames) and n is the number of monitor frames overlapping the imaging frame.

For the regression analysis in Figures 13-16, we then generated a matrix of fluorescence responses to individual resampled TF fluctuations by subtracting the baseline fluorescence at the onset of the monitor frame. We then computed regression coefficients of baseline corrected fluorescence against $\log_2$-transformed TF for each

time lag, only including fluorescence frames acquired during the baseline stimulus and at least 1 second prior to early licks or wheel movements.

We then quantified the timecourse of regression coefficients in different cortical areas by fitting a multiexponential model:

$$b(t) = b_{max}(1 - e^{-t/\tau_r})^z e^{-t/\tau_d}$$

Peak response b_{max}, power coefficient z, and rise and decay time constants τ_r and τ_d were optimized using *lsqnonlin* in MATLAB. The peak response in Figure 5C was directly given by the corresponding fit parameter. Response latency (Figure 5D) was estimated as the time lag, at which the multiexponential fit exceeded 50% of its maximum absolute value. The half decay time (Figure 5E) was estimated the as time following the response maximum at which the fit fell below 50% of its maximum value. If this did not occur within the 2 s window we analysed, half decay time is reported as not determined (N.D.).

For the analyses of responses to binned TF fluctuations in Figures 6-7, we computed mean fluorescence traces aligned to resampled TF fluctuations within each TF bin, again only including fluorescence frames acquired during the baseline stimulus and at least 1 second prior to early licks or wheel movements. To account for the overall timecourse of the baseline stimulus response (Figure 3), we then subtracted the mean response to the middle bin from responses to extreme bins. Due to the large sample size (tens to hundreds of thousands of imaging frames), confidence intervals

were computed using the Normal approximation from the standard errors of mean fluorescence responses in each bin.

8.9. Videography data extraction

Right eye was illuminated with custom made IR-light source and imaged using CMOS camera (DMK22BUC03, Imaging Source, ~30 Hz). Frames were filtered using 2-D gaussian filter (σ=2) and thresholded to low IR light reflectance areas (< 7.5 % image max intensity). Regions were filtered based on circularity (perimeter squared to area ratio < 1.6 x 4π) and size (>100 pixels). Edges of the area were detected using canny method and filtered using a Gaussian filter (σ=1). Ellipse was fitted iteratively to the region matching the criteria by minimizing the geometric distance between the area outline and the fitted ellipse using nonlinear least squares (MATLAB function *fitellipse*, Dr. Richard Brown) based on parameters returned by *regionprops* function in MATLAB. Z-scored major ellipse axis was taken as pupil diameter. Second CMOS camera was placed in front of the animal capturing animals' face and body. Body motion was expressed as the mean squared difference between the two consecutive frames.

References

Akrami, A., Kopec, C.D., Diamond, M.E., and Brody, C.D., 2018. Posterior parietal cortex represents sensory history and mediates its effects on behaviour. *Nature*, 554 (7692), 368–372.

Allen, W.E., Kauvar, I. V., Chen, M.Z., Richman, E.B., Yang, S.J., Chan, K., Gradinaru, V., Deverman, B.E., Luo, L., and Deisseroth, K., 2017. Global Representations of Goal-Directed Behavior in Distinct Cell Types of Mouse Neocortex. *Neuron*, 94 (4), 891-907.e6.

Andermann, M.L., Kerlin, A.M., and Reid, R.C., 2010. Chronic cellular imaging of mouse visual cortex during operant behavior and passive viewing. *Frontiers in Cellular Neuroscience*, 4 (MAR).

Andermann, M.L., Kerlin, A.M., Roumis, D.K., Glickfeld, L.L., and Reid, R.C., 2011. Functional Specialization of Mouse Higher Visual Cortical Areas. *Neuron*, 72 (6), 1025–1039.

Attinger, A., Wang, B., and Keller, G.B., 2017. Visuomotor Coupling Shapes the Functional Development of Mouse Visual Cortex. *Cell*, 169 (7), 1291-1302.e14.

Babayan, B.M. and Konen, C.S., 2019. Behavior Matters. *Neuron*, 104 (1), 1.

Barthas, F. and Kwan, A.C., 2017. Secondary Motor Cortex: Where 'Sensory' Meets 'Motor' in the Rodent Frontal Cortex. *Trends in Neurosciences*.

Bennur, S. and Gold, J.I., 2011. Distinct representations of a perceptual decision and the associated oculomotor plan in the monkey lateral intraparietal area. *The Journal of neuroscience : the official journal of the Society for Neuroscience*, 31 (3), 913–21.

Britten, K.H., Newsome, W.T., Shadlen, M.N., Celebrini, S., and Movshon, J.A., 1996. A relationship between behavioral choice and the visual responses of neurons in macaque MT. *Visual Neuroscience*, 13 (1), 87–100.

Britten, K.H., Shadlen, M.N., Newsome, W.T., and Movshon, J.A., 1993. Responses of neurons in macaque MT to stochastic motion signals. *Visual Neuroscience*,

10 (6), 1157–1169.

Burgess, C.P., Lak, A., Steinmetz, N.A., Zatka-Haas, P., Bai Reddy, C., Jacobs, E.A.K., Linden, J.F., Paton, J.J., Ranson, A., Schröder, S., Soares, S., Wells, M.J., Wool, L.E., Harris, K.D., and Carandini, M., 2017. High-Yield Methods for Accurate Two-Alternative Visual Psychophysics in Head-Fixed Mice. *Cell Reports*, 20 (10), 2513–2524.

Carandini, M. and Churchland, A.K., 2013. Probing perceptual decisions in rodents. *Nature Neuroscience*.

Churchland, M.M., Cunningham, J.P., Kaufman, M.T., Ryu, S.I., and Shenoy, K. V, 2010. Cortical Preparatory Activity: Representation of Movement or First Cog in a Dynamical Machine? *Neuron*, 68 (3), 387–400.

Crapse, T.B. and Sommer, M.A., 2008. Corollary discharge across the animal kingdom. *Nature Reviews Neuroscience*.

Dadarlat, M.C. and Stryker, M.P., 2017. Locomotion enhances neural encoding of visual stimuli in mouse V1. *Journal of Neuroscience*, 37 (14), 3764–3775.

Dana, H., Chen, T.W., Hu, A., Shields, B.C., Guo, C., Looger, L.L., Kim, D.S., and Svoboda, K., 2014. Thy1-GCaMP6 transgenic mice for neuronal population imaging in vivo. *PLoS ONE*, 9 (9).

Ding, L. and Gold, J.I., 2010. Caudate Encodes Multiple Computations for Perceptual Decisions. *Journal of Neuroscience*, 30 (47), 15747–15759.

Dipoppa, M., Ranson, A., Krumin, M., Pachitariu, M., Carandini, M., and Harris, K.D., 2018. Vision and Locomotion Shape the Interactions between Neuron Types in Mouse Visual Cortex. *Neuron*, 98 (3), 602-615.e8.

Donders, F.C., 1969. On the speed of mental processes. *Acta Psychologica*, 30, 412–431.

Ebbesen, C.L., Insanally, M.N., Kopec, C.D., Murakami, M., Saiki, A., and Erlich, J.C., 2018. More than just a “motor”: Recent surprises from the frontal cortex. *Journal of Neuroscience*, 38 (44), 9402–9413.

Economo, M.N., Viswanathan, S., Tasic, B., Bas, E., Winnubst, J., Menon, V., Graybuck, L.T., Nguyen, N., Smith, K.A., Yao, Z., Wang, L., Gerfen, C.R.,

Chandrashekar, J., Zeng, H., Looger, L.L., Svoboda, K., Nguyen, T.N., Smith, K.A., Yao, Z., Wang, L., Gerfen, C.R., Chandrashekar, J., Zeng, H., Looger, L.L., and Svoboda, K., 2018. Distinct descending motor cortex pathways and their roles in movement. *Nature*, 563 (7729), 79–84.

Fee, M.S., 2014. The role of efference copy in striatal learning. *Curr Opin Neurobiol*, 25, 194–200.

Fiser, A., Mahringer, D., Oyibo, H.K., Petersen, A. V., Leinweber, M., and Keller, G.B., 2016. Experience-dependent spatial expectations in mouse visual cortex. *Nature Neuroscience*, 19 (12), 1658–1664.

Fu, Y., Tucciarone, J.M., Espinosa, J.S., Sheng, N., Darcy, D.P., Nicoll, R.A., Huang, Z.J., and Stryker, M.P., 2014. A cortical circuit for gain control by behavioral state. *Cell*, 156 (6), 1139–1152.

Gao, Z., Davis, C., Thomas, A.M., Economo, M.N., Abrego, A.M., Svoboda, K., De Zeeuw, C.I., and Li, N., 2018. A cortico-cerebellar loop for motor planning. *Nature*.

Garcia Del Molino, L.C., Yang, G.R., Mejias, J.F., and Wang, X.J., 2017. Paradoxical response reversal of top- down modulation in cortical circuits with three interneuron types. *eLife*, 6.

Gold, J.I. and Shadlen, M.N., 2000. Representation of a perceptual decision in developing oculomotor commands. *Nature*, 404 (6776), 390–394.

Gold, J.I. and Shadlen, M.N., 2001. Neural computations that underlie decisions about sensory stimuli. *Trends in Cognitive Sciences*.

Gold, J.I. and Shadlen, M.N., 2002. Banburismus and the Brain: Decoding the Relationship between Sensory Stimuli, Decisions, and Reward. *Neuron*, 36 (2), 299–308.

Gold, J.I. and Shadlen, M.N., 2007. The Neural Basis of Decision Making.

Gomez-Marin, A. and Ghazanfar, A.A., 2019. The Life of Behavior. *Neuron*, 104 (1), 25–36.

Grinvald, A., Lieke, E., Frostig, R.D., Gilbert, C.D., Wiesel, T.N., Madsen, I., and Bull, J.H., 1976. *Functional architecture of cortex revealed by optical imaging*

of intrinsic signals. Taquet, P. Cr. hebd. Sianc. Acad. Sci.

Guo, Z. V., Inagaki, H.K., Daie, K., Druckmann, S., Gerfen, C.R., and Svoboda, K., 2017. Maintenance of persistent activity in a frontal thalamocortical loop. *Nature*, 545 (7653), 181–186.

Guo, Z. V., Li, N., Huber, D., Ophir, E., Gutnisky, D., Ting, J.T., Feng, G., and Svoboda, K., 2014. Flow of cortical activity underlying a tactile decision in mice. *Neuron*, 81 (1), 179–194.

Han, Y., Kebschull, J.M., Campbell, R.A.A., Cowan, D., Imhof, F., Zador, A.M., and Mrsic-Flogel, T.D., 2018. The logic of single-cell projections from visual cortex. *Nature*, 556 (7699), 51–56.

Hangya, B., Ranade, S.P., Lorenc, M., and Kepecs, A., 2015. Central Cholinergic Neurons Are Rapidly Recruited by Reinforcement Feedback. *Cell*, 162 (5), 1155–1168.

Hanks, T.D. and Summerfield, C., 2017. Perceptual Decision Making in Rodents, Monkeys, and Humans. *Neuron*.

Harvey, C.D., Coen, P., and Tank, D.W., 2012. Choice-specific sequences in parietal cortex during a virtual-navigation decision task. *Nature*, 484 (7392), 62–68.

Heindorf, M., Arber, S., and Keller, G.B., 2018. Mouse Motor Cortex Coordinates the Behavioral Response to Unpredicted Sensory Feedback. *Neuron*, 99 (5), 1040-1054.e5.

Hernández, A., Nácher, V., Luna, R., Zainos, A., Lemus, L., Alvarez, M., Vázquez, Y., Camarillo, L., and Romo, R., 2010. Decoding a perceptual decision process across cortex. *Neuron*, 66 (2), 300–314.

Hernandez, A., Zainos, A., and Romo, R., 2000. Neuronal correlates of sensory discrimination in the somatosensory cortex. *Proceedings of the National Academy of Sciences*, 97 (11), 6191–6196.

Hernández, A., Zainos, A., and Romo, R., 2002. Temporal evolution of a decision-making process in medial premotor cortex. *Neuron*, 33 (6), 959–972.

Hintiryan, H., Foster, N.N., Bowman, I., Bay, M., Song, M.Y., Gou, L., Yamashita, S., Bienkowski, M.S., Zingg, B., Zhu, M., Yang, X.W., Shih, J.C., Toga, A.W.,

and Dong, H.W., 2016. The mouse cortico-striatal projectome. *Nature Neuroscience*, 19 (8), 1100–1114.

Hooks, B.M., Mao, T., Gutnisky, D.A., Yamawaki, N., Svoboda, K., and Shepherd, G.M.G., 2013. Organization of cortical and thalamic input to pyramidal neurons in mouse motor cortex. *Journal of Neuroscience*, 33 (2), 748–760.

Huang, Z.J. and Zeng, H., 2013. Genetic Approaches to Neural Circuits in the Mouse. *Annual Review of Neuroscience*, 36 (1), 183–215.

Huber, D., Petreanu, L., Ghitani, N., Ranade, S., Hromádka, T., Mainen, Z., and Svoboda, K., 2008. Sparse optical microstimulation in barrel cortex drives learned behaviour in freely moving mice. *Nature*, 451 (7174), 61–64.

Huk, A.C. and Shadlen, M.N., 2005. Behavioral/Systems/Cognitive Neural Activity in Macaque Parietal Cortex Reflects Temporal Integration of Visual Motion Signals during Perceptual Decision Making.

Huk, X.A., Bonnen, K., Biyu, X., and He, J., 2018. Beyond Trial-Based Paradigms: Continuous Behavior, Ongoing Neural Activity, and Natural Stimuli.

Hwang, E.J., Dahlen, J.E., Mukundan, M., and Komiyama, T., 2017. History-based action selection bias in posterior parietal cortex. *Nature Communications*, 8 (1).

Jaramillo, S. and Zador, A.M., 2011. The auditory cortex mediates the perceptual effects of acoustic temporal expectation. *Nature Neuroscience*, 14 (2), 246–251.

Juavinett, A.L., Erlich, J.C., and Churchland, A.K., 2018. Decision-making behaviors: weighing ethology, complexity, and sensorimotor compatibility. *Current Opinion in Neurobiology*.

Katz, L.N., Yates, J.L., Pillow, J.W., and Huk, A.C., 2016. Dissociated functional significance of decision-related activity in the primate dorsal stream. *Nature*, 535 (7611), 285–288.

Kaufman, M.T., Churchland, M.M., Ryu, S.I., and Shenoy, K. V, 2014. Cortical activity in the null space: permitting preparation without movement. *Nature Publishing Group*, 17.

Keller, G.B., Bonhoeffer, T., and Hübener, M., 2012. Sensorimotor Mismatch Signals in Primary Visual Cortex of the Behaving Mouse. *Neuron*, 74 (5), 809–

815.

Khibnik, L.A., Tritsch, N.X., and Sabatini, B.L., 2014. A direct projection from mouse primary visual cortex to dorsomedial striatum. *PLoS ONE*, 9 (8).

Kim, J.-N.N. and Shadlen, M.N., 1999. *Neural correlates of a decision in the dorsolateral prefrontal cortex of the macaque*. Nature Neuroscience.

Klein, S., Staring, M., Murphy, K., Viergever, M.A., and Pluim, J.P.W., 2010. Elastix: A toolbox for intensity-based medical image registration. *IEEE Transactions on Medical Imaging*, 29 (1), 196–205.

Kleiner, M., Brainard, D., and Pelli, D., 2007. What's new in Psychtoolbox-3? *In*: *Perception ECVP Abstract Supplement*. Pion Ltd, 0.

Krakauer, J.W., Ghazanfar, A.A., Gomez-Marin, A., MacIver, M.A., and Poeppel, D., 2017. Neuroscience Needs Behavior: Correcting a Reductionist Bias. *Neuron*, 93 (3), 480–490.

Krumin, M., Lee, J.J., Harris, K.D., and Carandini, M., 2018. Decision and navigation in mouse parietal cortex. *eLife*, 7.

Kunimatsu, J., Suzuki, T.W., Ohmae, S., and Tanaka, M., 2018. Different contributions of preparatory activity in the basal ganglia and cerebellum for self-timing. *eLife*, 7.

de Lafuente, V. and Romo, R., 2006. Neural correlate of subjective sensory experience gradually builds up across cortical areas. *Proceedings of the National Academy of Sciences*, 103 (39), 14266 LP – 14271.

Leinweber, M., Ward, D.R., Sobczak, J.M., Attinger, A., and Keller, G.B., 2017. A Sensorimotor Circuit in Mouse Cortex for Visual Flow Predictions. *Neuron*, 95 (6), 1420-1432.e5.

Lerner, T.N., Shilyansky, C., Davidson, T.J., Evans, K.E., Beier, K.T., Zalocusky, K.A., Crow, A.K., Malenka, R.C., Luo, L., Tomer, R., and Deisseroth, K., 2015. Intact-Brain Analyses Reveal Distinct Information Carried by SNc Dopamine Subcircuits. *Cell*, 162 (3), 635–647.

Li, N., Chen, T.W., Guo, Z. V, Gerfen, C.R., and Svoboda, K., 2015. A motor cortex circuit for motor planning and movement. *Nature*, 519 (7541), 51–56.

Luo, L., Callaway, E.M., and Svoboda, K., 2018. Genetic Dissection of Neural Circuits: A Decade of Progress. *Neuron*.

Ma, Y., Shaik, M.A., Kim, S.H., Kozberg, M.G., Thibodeaux, D.N., Zhao, H.T., Yu, H., and Hillman, E.M.C., 2016. Wide-field optical mapping of neural activity and brain haemodynamics: Considerations and novel approaches. *Philosophical Transactions of the Royal Society B: Biological Sciences*.

Makino, H., Ren, C., Liu, H., Kim, A.N., Kondapaneni, N., Liu, X., Kuzum, D., and Komiyama, T., 2017. Transformation of Cortex-wide Emergent Properties during Motor Learning. *Neuron*, 94 (4), 880-890.e8.

Marshel, J.H., Garrett, M.E., Nauhaus, I., and Callaway, E.M., 2011. Functional Specialization of Seven Mouse Visual Cortical Areas. *Neuron*, 72 (6), 1040–1054.

Mazurek, M.E., Roitman, J.D., Ditterich, J., and Shadlen, M.N., 2003. A Role for Neural Integrators in Perceptual Decision Making. *Cerebral Cortex*.

Mobbs, D., Trimmer, P.C., Blumstein, D.T., and Dayan, P., 2018. Foraging for foundations in decision neuroscience: Insights from ethology. *Nature Reviews Neuroscience*.

Mountcastle, V.B., Steinmetz, M.A., and Romo, R., 1990. Frequency discrimination in the sense of flutter: psychophysical measurements correlated with postcentral events in behaving monkeys. *The Journal of Neuroscience*, 10 (9), 3032 LP – 3044.

Murakami, M. and Mainen, Z.F., 2015. Preparing and selecting actions with neural populations: toward cortical circuit mechanisms. *Current Opinion in Neurobiology*, 33, 40–46.

Musall, S., Kaufman, M.T., Juavinett, A.L., Gluf, S., and Churchland, A.K., 2019. Single-trial neural dynamics are dominated by richly varied movements. *Nature Neuroscience*, 22 (10), 1677–1686.

Newsome, W.T., Britten, K.H., and Movshon, J.A., 1989. Neuronal correlates of a perceptual decision. *Nature*, 341 (6237), 52–54.

Newsome, W.T. and Pare, E.B., 1988. A selective impairment of motion perception following lesions of the middle temporal visual area (MT). *Journal of*

Neuroscience, 8 (6), 2201–2211.

Niell, C.M. and Stryker, M.P., 2010. Modulation of Visual Responses by Behavioral State in Mouse Visual Cortex. *Neuron*, 65 (4), 472–479.

O'Connor, D.H., Clack, N.G., Huber, D., Komiyama, T., Myers, E.W., and Svoboda, K., 2010. Vibrissa-based object localization in head-fixed mice. *Journal of Neuroscience*, 30 (5), 1947–1967.

Odoemene, O., Pisupati, S., Nguyen, H., and Churchland, A.K., 2018. Visual evidence accumulation guides decision-making in unrestrained mice. *The Journal of neuroscience : the official journal of the Society for Neuroscience*, 3478–17.

Okazawa, G., Sha, L., Purcell, B.A., and Kiani, R., 2018. Psychophysical reverse correlation reflects both sensory and decision-making processes. *Nature Communications*, 9 (1), 3479.

Pinto, L., Koay, S.A., Engelhard, B., Yoon, A.M., Deverett, B., Thiberge, S.Y., Witten, I.B., Tank, D.W., and Brody, C.D., 2018. An accumulation-of-evidence task using visual pulses for mice navigating in virtual reality. *Frontiers in Behavioral Neuroscience*, 12.

Pinto, L., Rajan, K., DePasquale, B., Thiberge, S.Y., Tank, D.W., and Brody, C.D., 2019. Task-Dependent Changes in the Large-Scale Dynamics and Necessity of Cortical Regions. *Neuron*.

Poort, J., Khan, A.G., Pachitariu, M., Nemri, A., Orsolic, I., Krupic, J., Bauza, M., Sahani, M., Keller, G.B., Mrsic-Flogel, T.D., and Hofer, S.B., 2015. Learning Enhances Sensory and Multiple Non-sensory Representations in Primary Visual Cortex. *Neuron*, 86 (6), 1478–90.

Ratzlaff, E.H. and Grinvald, A., 1991. A tandem-lens epifluorescence macroscope: Hundred-fold brightness advantage for wide-field imaging. *Journal of Neuroscience Methods*, 36 (2–3), 127–137.

Roitman, J.D. and Shadlen, M.N., 2002. Response of neurons in the lateral intraparietal area during a combined visual discrimination reaction time task. *Journal of Neuroscience*, 22 (21), 9475–9489.

Romo, R., Hernández, A., Zainos, A., Brody, C.D., and Lemus, L., 2000. Sensing

without touching: Psychophysical performance based on cortical microstimulation. *Neuron*, 26 (1), 273–278.

Romo, R., Hernández, A., Zainos, A., and Salinas, E., 1998. Somatosensory discrimination based on cortical microstimulation. *Nature*, 392 (6674), 387–390.

Salzman, C.D., Britten, K.H., and Newsome, W.T., 1990. Cortical microstimulation influences perceptual judgements of motion direction. *Nature*, 346 (6280), 174–177.

Sanders, J.I. and Kepecs, A., 2012. Choice ball: A response interface for two-choice psychometric discrimination in head-fixed mice. *Journal of Neurophysiology*, 108 (12), 3416–3423.

Shadlen, M.N. and Newsome, W.T., 1996. Motion perception: Seeing and deciding. *Proceedings of the National Academy of Sciences of the United States of America*, 93 (2), 628–633.

Shenoy, K. V., Sahani, M., and Churchland, M.M., 2013. Cortical Control of Arm Movements: A Dynamical Systems Perspective. *Annual Review of Neuroscience*, 36 (1), 337–359.

Siegel, M., Buschman, T.J., and Miller, E.K., 2015. Cortical information flow during flexible sensorimotor decisions. *Science (New York, N.Y.)*, 348 (6241), 1352–5.

Silasi, G., Xiao, D., Vanni, M.P., Chen, A.C.N., and Murphy, T.H., 2016. Intact skull chronic windows for mesoscopic wide-field imaging in awake mice. *Journal of neuroscience methods*, 267, 141–9.

Steinmetz, N.A., Buetfering, C., Lecoq, J., Lee, C.R., Peters, A.J., Jacobs, E.A.K., Coen, P., Ollerenshaw, D.R., Valley, M.T., de Vries, S.E.J., Garrett, M., Zhuang, J., Groblewski, P.A., Manavi, S., Miles, J., White, C., Lee, E., Griffin, F., Larkin, J.D., Roll, K., Cross, S., Nguyen, T. V., Larsen, R., Pendergraft, J., Daigle, T., Tasic, B., Thompson, C.L., Waters, J., Olsen, S., Margolis, D.J., Zeng, H., Hausser, M., Carandini, M., and Harris, K.D., 2017. Aberrant Cortical Activity in Multiple GCaMP6-Expressing Transgenic Mouse Lines. *eneuro*.

Steinmetz, N.A., Zatka-Haas, P., Carandini, M., and Harris, K.D., 2018. Distributed correlates of visually-guided behavior across the mouse brain. *bioRxiv*, 474437.

Stringer, C., Pachitariu, M., Steinmetz, N., Reddy, C.B., Carandini, M., and Harris, K.D., 2019. Spontaneous behaviors drive multidimensional, brainwide activity. *Science*, 364 (6437).

Svoboda, K. and Li, N., 2018. Neural mechanisms of movement planning: motor cortex and beyond. *Current Opinion in Neurobiology*.

Tye, K.M. and Uchida, N., 2018. Editorial overview: Neurobiology of behavior New tools and behavioral paradigms. *Current Opinion in Neurobiology*, 49, xx-yy.

Wang, L., Rangarajan, K. V., Gerfen, C.R., and Krauzlis, R.J., 2018. Activation of Striatal Neurons Causes a Perceptual Decision Bias during Visual Change Detection in Mice. *Neuron*, 97 (6), 1369-1381.e5.

Waskom, M.L., Okazawa, G., and Kiani, R., 2019. Designing and Interpreting Psychophysical Investigations of Cognition. *Neuron*, 104 (1), 100–112.

Wekselblatt, J.B., Flister, E.D., Piscopo, D.M., and Niell, C.M., 2016. Large-scale imaging of cortical dynamics during sensory perception and behavior. *Journal of Neurophysiology*.

Werner, G. and Mountcastle, V.B., 1965. Neural activity in mechanoreceptive cutaneous afferents: Stimulus-response relations, Weber functions, and information transmission. *Journal of neurophysiology*, 28, 359–397.

Winnubst, J., Bas, E., Ferreira, T.A., Spruston, N., Svoboda, K., Chandrashekar, J., Winnubst, J., Bas, E., Ferreira, T.A., Wu, Z., Economo, M.N., Edson, P., Arthur, B.J., Bruns, C., Rokicki, K., Schauder, D., Olbris, D.J., Murphy, S.D., Ackerman, D.G., Santos, B. Dos, Weldon, M., Zafar, A., Dudman, J.T., Gerfen, C.R., and Hantman, A.W., 2019. Reconstruction of 1 , 000 Projection Neurons Reveals New Cell Types and Organization of Long-Range Connectivity in the Mouse Brain Resource Reconstruction of 1 , 000 Projection Neurons Reveals New Cell Types and Organization of Long-Range Connectivity in . *Cell*, 1–14.

Wolpert, D.M. and Landy, M.S., 2012. Motor Control is Decision-Making.

Wong, A.L., Haith, A.M., and Krakauer, J.W., 2015. Motor Planning. *The Neuroscientist*, 21 (4), 385–398.

Zatka-Haas, P., Steinmetz, N.A., Carandini, M., and Harris, K.D., 2018. Distinct contributions of mouse cortical areas to visual discrimination. *bioRxiv*, 501627.

Zhang, S., Xu, M., Chang, W.C., Ma, C., Hoang Do, J.P., Jeong, D., Lei, T., Fan, J.L., and Dan, Y., 2016. Organization of long-range inputs and outputs of frontal cortex for top-down control. *Nature Neuroscience*, 19 (12), 1733–1742.

Znamenskiy, P. and Zador, A.M., 2013. Corticostriatal neurons in auditory cortex drive decisions during auditory discrimination. *Nature*, 497 (7450), 482–485.